

Novel scaling law governing stock price dynamics

Hideyuki Miyahara,^{*} Hai Qian, Pavan Holur, and Vwani Roychowdhury[†]

*Department of Electrical and Computer Engineering,
University of California, Los Angeles, California 90095*

A stock market is typically modeled as a complex system where the purchase, holding or selling of individual stocks affects other stocks in nonlinear and collaborative ways that cannot be always captured using succinct models. Such complexity arises due to several latent and confounding factors, such as variations in decision making because of incomplete information, and differing short/long-term objectives of traders. While few emergent phenomena such as seasonality and fractal behaviors in individual stock price data have been reported, universal scaling laws that apply collectively to the market are rare. In this paper, we consider the market-mode adjusted pairwise correlations of returns over different time scales (τ), $c_{i,j}(\tau)$, and discover two such novel emergent phenomena: (i) the standard deviation of the $c_{i,j}(\tau)$'s scales as $\tau^{-\lambda}$, for τ larger than a certain return horizon, τ_0 , where λ is the scaling exponent, (ii) moreover, the scaled and zero-shifted distributions of the $c_{i,j}(\tau)$'s are invariant of $\tau > \tau_0$. Our analysis of S&P500 market data collected over almost 20 years (2004 – 2020) demonstrates that the twin scaling property holds for each year and across 2 decades (orders of magnitude) of τ . Moreover, we find that the scaling exponent λ provides a summary view of market volatility: in years marked by unprecedented financial crises – for example 2008 and 2020 – values of λ are substantially higher. As for analytical modeling, we demonstrate that such scaling behaviors observed in data cannot be explained by existing theoretical frameworks such as the single- and multi-factor models. To close this gap, we introduce a promising agent-based model – inspired by literature on swarming – that displays more of the emergent behaviors exhibited by the real market data.

I. INTRODUCTION

Commodity prices in a stock market demonstrate considerable volatility, a result of several compounding factors such as traders' collaborative and competitive decision-making to buy, hold or sell, differing appetites for risk, and various time horizons for expected returns on investment [1–7]. A considerable body of literature has focused on identifying patterns in commodity price fluctuations and on developing succinct dynamical models that display similar characteristics as a real market. Financial experts have, for instance, frequently observed seasonality patterns in stock prices and the fractal nature of price fluctuations [8, 9]. However, macroscopic patterns – those patterns that apply on the entire market or a market sector – are rare but highly desired: researchers constantly pursue universal laws that govern market growth, volatility and crises. Oftentimes, models that are proposed to explain these observations are derived from the abundant literature in swarming and econophysics [10, 11]. In these approaches, the stock market is viewed as a closed environment, where individual stocks behave as agents that influence other agents. At each time-step, the position of an agent corresponds to a particular stock's instantaneous market behavior. Agents that exhibit correlated trajectories over multiple time steps often cluster together behaving as swarms. In the context of a stock market, such swarms can be likened to different GICS sectors [12].

In order to numerically model the dynamics of such groups in a market, one needs to define a financially-relevant similarity metric involving the time series sequences of stock prices. An investor evaluates the performance of a stock based on returns, which over a time horizon of τ is computed as the logarithm of the ratio of the stock's price at time $t + \tau$ to its price at time t . The pairwise correlations of return sequences are therefore a suitable similarity metric to compare stocks' performances over time [4]. One can now map the entire market to a fully-connected network – a consensus representation – where the stocks are nodes and the pair-wise correlations correspond to the inter-stock edge weights. Structures are distilled from within the network representation by adopting various graph theory algorithms [13–16].

In this paper, we first revisit one popular method to extract structure from the consensus network representation that involves computing the Minimum Spanning Tree (MST). In accordance to earlier work, we observe that the MST possesses a vine-like structure (see Fig. 1) that is dependent on the choice of the time horizon τ . This motivates the question, “Are there *quantifiable* patterns and *summary* statistics in the correlation matrix as a whole, wherein the

^{*} miyahara@g.ucla.edu, hmiyahara512@gmail.com; Current affiliation: Graduate School of Information Science and Technology, Hokkaido University, Sapporo, Hokkaido, 060-0814, Japan

[†] vwani@ucla.edu; Corresponding Author

vine structure observed so far in the MSTs are just but one identified outcome?" Such phenomena that vary as a function of τ are indispensable to investors constructing a well-balanced portfolio.

Any emergent market dynamics would be reflected in the correlation patterns and a fundamental macroscopic observable is the distribution of the entire set of pairwise return correlations: the functional form of the probability density function and how different statistics of the density functions evolve as a function of time horizon τ . Patterns in such summary statistics often carry telltale signature of the underlying dynamics, helping researchers to formulate succinct generative models, which in turn can be used to stabilize or steer the marketplace in desirable directions. Before estimating the density functions, we subtract the average correlations that emerge due to overall market fluctuations, referred to as the *market mode*. Debiasing the correlations in this way highlights the interaction dynamics amongst the stocks. The residuals, $c_{i,j}(\tau)$'s, are termed *market-mode adjusted* correlations.

We discover a robust universal scaling law that governs the standard deviation of $c_{i,j}(\tau)$ with respect to the return horizon parameter τ ; i.e for $\tau > \tau_0$, the standard deviation of the $c_{i,j}(\tau)$'s scales as $\tau^{-\lambda}$, where $\lambda > 0$ is the scaling exponent. In the region $\tau > \tau_0$, the scaled and zero-shifted distributions of the $c_{i,j}(\tau)$'s is invariant of $\tau > \tau_0$. The scaling law holds across nearly two decades of τ . The data used to validate the discovered emergent phenomena includes 17 years of S&P500 prices for each of the ~ 500 symbols sampled every minute. Data can be accessed at the Wharton Research Data Services (WRDS)[17] and the code repository [18] is linked [19].

Finally, we reexamine the single- and multi-factor generative models, popular choices considered today while modeling consensus behavior in financial markets. These models for the most part fail to replicate the above mentioned emergent trends – including the scaling law: (a) The single-factor model fails to reproduce the vine MST structure; (b) Multi-factor models, on the other hand, can generate the vine; however, fail to reproduce the scaling law. To close this gap, we propose an alternate framework – a modified Vicsek model commonly used to describe the dynamics of active matter – that more reliably reproduces the observed emergent phenomena.

II. PREREQUISITES

A. Conventional correlation, market correlation and market-mode adjusted correlation

Suppose a market has N stocks; in the S&P500, $N \approx 500$. Let us denote, by $p_i(t)$, the price of stock i at time t for $i = 1, 2, \dots, N$ and $t_{\text{ini}} \leq t \leq t_{\text{fin}}$. In many macroeconomic market analyses, $T_{\text{int}} := t_{\text{fin}} - t_{\text{ini}}$ is limited to 1 year from January 1st to December 31 since this window mitigates seasonality patterns observed in longer series: a consequence of the periodic expanding and contracting phases of demand for commodities depending on the financial quarter. Indeed, many existing measures of market health are tracked per year: year-over-year (YoY) gain, annualized returns and even, yearly GDP growth.

A key metric used by investors in order to evaluate the relative performance of a stock within the T_{int} window is the effective return or interest rate of the stock over a time horizon of τ ($\tau \leq T_{\text{int}}$). A common definition of such return $r_i(t; \tau)$ of a stock at time t over a period of τ is: the interest rate such that an investment in the i^{th} stock at time t (say, a sum of $mp_i(t)$ by purchasing m units) when *compounded continuously* at the given rate would yield the same amount as that would be obtained by selling the stock at time $(t + \tau)$ (i.e., $mp_i(t + \tau)$). Quantitatively,

$$mp_i(t + \tau) = mp_i(t) \lim_{n \rightarrow \infty} \left(1 + \frac{r_i(t; \tau)}{n\tau} \right)^{n\tau} = mp_i(t) e^{r_i(t; \tau)}. \quad \text{Thus, we get:}$$

$$r_i(t; \tau) := \ln p_i(t + \tau) - \ln p_i(t), \quad (\text{II.1.1})$$

for $t_{\text{ini}} \leq t \leq t_{\text{fin}} - \tau$. Therefore, an investment horizon of τ yields a return sequence of length, $T_{\text{int}} - \tau + 1$.

The correlations between these return sequences are debiased by subtracting the correlations with respect to the market as a whole. As discussed earlier, subtracting the market mode helps highlight the correlations between pairs of stock. The interest rate of the market using the collection of all the return sequences $r_i(\cdot; \tau)$ is defined: for $t_{\text{ini}} \leq t \leq t_{\text{fin}} - \tau$,

$$r_0(t; \tau) := \frac{1}{N} \sum_{i=1}^N r_i(t; \tau). \quad (\text{II.1.2})$$

We denote the time average of $r_i(\cdot; \tau)$ and $r_i(\cdot; \tau)r_j(\cdot; \tau)$ for $i, j = 0, 1, 2, \dots, N$ by

$$\overline{r_i(\cdot; \tau)} := \int_{t_{\text{ini}}}^{t_{\text{fin}} - \tau} dt r_i(t; \tau), \quad (\text{II.1.3})$$

$$\overline{r_i(\cdot; \tau)r_j(\cdot; \tau)} := \int_{t_{\text{ini}}}^{t_{\text{fin}} - \tau} dt r_i(t; \tau)r_j(t; \tau). \quad (\text{II.1.4})$$

For $i, j = 0, 1, 2, \dots, N$, we define

$$\rho_{i,j}(\tau) := \frac{\sigma_{i,j}(\tau)}{\sigma_i(\tau)\sigma_j(\tau)}, \quad (\text{II.1.5})$$

where

$$\sigma_i(\tau) := \sqrt{r_i^2(\cdot; \tau) - \overline{r_i(\cdot; \tau)}^2}, \quad (\text{II.1.6})$$

$$\sigma_{i,j}(\tau) := \overline{r_i(\cdot; \tau)r_j(\cdot; \tau) - \overline{r_i(\cdot; \tau)} \cdot \overline{r_j(\cdot; \tau)}}. \quad (\text{II.1.7})$$

We call $\rho_{i,j}(\tau)$ in Eq. (II.1.5) the *conventional correlation*. With this definition, the correlation between stocks i and j with respect to the market mode is $\rho_{i,0}(\tau)\rho_{j,0}(\tau)$; this is the *market correlation*. More generally, one can measure the cross-correlation of $r_i(t)$ and $r_j(t + \Delta)$ by replacing the right-hand side of Eq. (II.1.4) by

$$\int_{t_{\text{ini}}}^{t_{\text{fin}} - \tau - \Delta} dt r_i(t; \tau) r_j(t + \Delta; \tau). \quad (\text{II.1.8})$$

Note: The correlation for non-zero time lag Δ should be equal to 0; otherwise the agents in the stock market would be able to use one stock return time series to predict another stock's return. So we set $\Delta = 0$.

Then, for $i, j = 1, 2, \dots, N$, the deviation of the conventional correlation from the market correlation between a pair of stocks i and j is given by:

$$c_{i,j}(\tau) := \rho_{i,j}(\tau) - \rho_{i,0}(\tau)\rho_{j,0}(\tau). \quad (\text{II.1.9})$$

Note that $\{c_{i,j}(\tau)\}_{i,j=1}^N$ in Eq. (II.1.9) describes the residual correlation between stocks i and j that *cannot* be represented by the market mode - this is the *market-mode adjusted correlation*.

B. Histograms, scaling function, and scaled histogram

The histogram of $\{c_{i,j}(\tau)\}_{i,j=1}^N$ is given by,

$$p_\tau(x) := \frac{1}{N^2} \sum_{i,j=1}^N \delta_D(x - c_{i,j}(\tau)), \quad (\text{II.2.1})$$

where $\delta_D(\cdot)$ is the Dirac delta function. Let $b(\tau)$ be the inverse of the standard deviation of $p_\tau(\cdot)$. Then, the scaled variant of $p_\tau(\cdot)$ in Eq. (II.2.1) is given by,

$$\tilde{p}_\tau(x) := \frac{1}{b(\tau)} p_\tau\left(\frac{x - \delta(\tau)}{b(\tau)}\right). \quad (\text{II.2.2})$$

We identify a scaling law that governs $b(\tau)$ as a function of τ while the shape of \tilde{p}_τ remains constant; i.e

$$b(\tau) = \tau^\lambda. \quad (\text{II.2.3})$$

λ is a critical parameter called the *exponent* and is often used to characterize dynamical systems.

III. EMPIRICAL RESULTS: EMERGENT PHENOMENA IN REAL-WORLD DATA

Consistent with existing macroeconomic financial indicators, we set $T_{\text{int}} = 1$ year in the main text. Analyses with smaller T_{int} s of 1, 3, 6 months are presented in the SM Section S-I. The results presented below are largely consistent with the shorter window analyses: however, since a smaller T_{int} implies a shorter series of returns, the computed correlations between these series – and observed emergent trends – are noisy in comparison to experiments that are performed using longer windows. The sampling time interval of stock prices is 1 minute. There are ~ 251 business days in a year when the stock market is open from 9 : 30 to 16 : 00 ET. For $T_{\text{int}} = 1$ year, this spans a ~ 98000 -length price series.

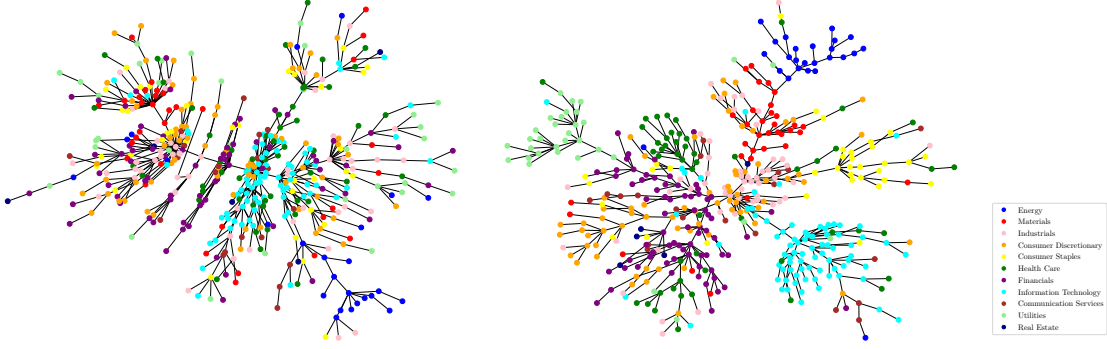


FIG. 1. MSTs with (left) $\tau = 1$ min and (right) $\tau = 1000$ min in 2004. The starting and end dates are Jan 1st and Dec 31st, respectively. The weights between stocks are defined by Eq. (III.1.1). Each vertex is colored depending on its GICS sector. Observe that for larger values of τ , stocks belonging to the same sector cluster together.

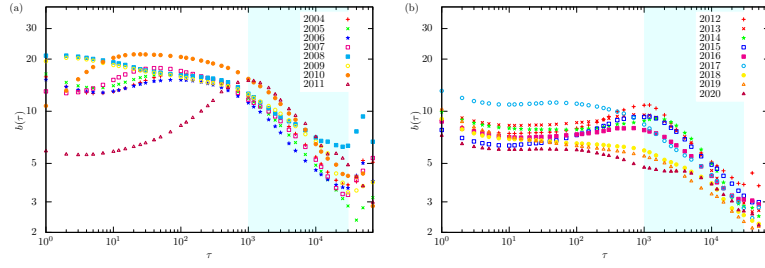


FIG. 2. Dependence of the scaling factor $b(\tau)$ on τ : (a) from 2004 to 2011; and (b) from 2012 to 2020. From $\tau = 1000$ min to 30000 min (the regime highlighted by light cyan), observe the linear relationship between $\ln \tau$ and $\ln b$. This is visual evidence of the scaling regime.

A. Exploring the structure of the stock market using minimum spanning trees

Following established approaches [20, 21], MSTs are constructed to represent the total S&P500 market where the nodes are stocks and the edge lengths are a function of the correlations $\rho_{i,j}(\tau)$:

$$d_{i,j}(\tau) := \sqrt{2(1 - \rho_{i,j}(\tau))}. \quad (\text{III.1.1})$$

In Fig. 1, the MSTs for the year 2004 with $\tau = 1$ min and $\tau = 1000$ min are shown. Observe: (a) Stocks belonging to the same sectors are less likely to belong to the same community for $\tau = 1$ min than $\tau = 1000$ min; (b) the vine structure of the MST is expressed more clearly for $\tau = 1000$ min than $\tau = 1$ min. In a qualitative sense, it is evident that the structure of the MST varies as a function of τ . In the next section, we will see that the full distribution of correlations as well varies with respect to τ .

B. The scaling law and its emergent properties

In Fig. 2 we plot the discovered scaling property of $b(\tau)$ with different τ from 2004 to 2020 (see SM Section S-I for experiments and results with $T_{int} < 1$ year). From $\tau = 1000$ min to 30000 min (the regime highlighted by light cyan), we observe a linear relationship between $\ln \tau$ and $\ln b$. Recall that $b(\tau)$ is the inverse of the standard deviation of the histogram of correlations of market-mode adjusted returns $p_\tau(x)$.

We additionally observe that during the scaling regime, the functional form of $\tilde{p}_\tau(\cdot)$ is independent of τ . In Figs. 3, 4, we emphasize this stable structure qualitatively for 2004 and 2012 by superimposing the functions $\tilde{p}_\tau(\cdot)$ across different τ . Similar plots for other years are presented in Figs. S-25 and S-26 in the SM. We quantify the similarity between the scaled distributions $p_\tau(\cdot)$ across different τ using:

- **Pairwise KL divergence between scaled correlation histograms:** For each year from 2004 to 2020, we compute the KL divergence (KLD) between $\tilde{p}_{\tau_1}(\cdot)$ and $\tilde{p}_{\tau_2}(\cdot)$, the scaled correlation histograms computed with

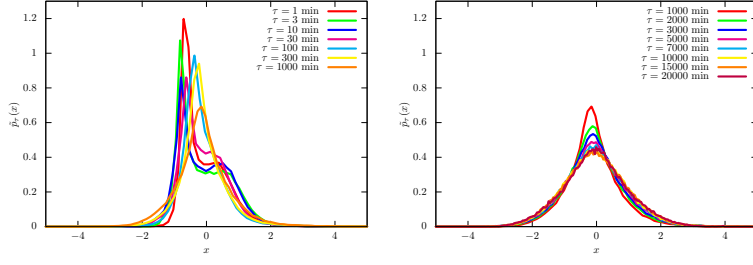


FIG. 3. Scaled histogram $\tilde{p}_\tau(\cdot)$ in Eq. (II.2.2) in 2004. (a) $\tau = 1$ min to 1000 min and (b) $\tau = 1000$ min to 30000 min. As τ exceeds 1000 min, the shape of $\tilde{p}_\tau(\cdot)$ takes a more stable form.

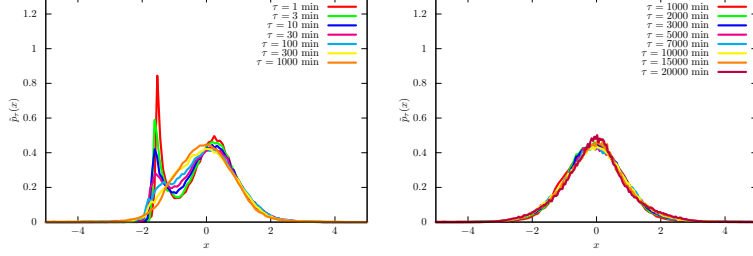


FIG. 4. Scaled histogram $\tilde{p}_\tau(\cdot)$ in Eq. (II.2.2) in 2012. (a) $\tau = 1$ min to 1000 min and (b) $\tau = 1000$ min to 30000 min. As τ exceeds 1000 min, the shape of $\tilde{p}_\tau(\cdot)$ stabilizes similar to the results in Fig. 3.

τ_1 and τ_2 respectively. We would like to show that in the scaling regime ($1000 \leq \tau \leq 30000$), $D_{KL}(\tilde{p}_{\tau_1} || \tilde{p}_{\tau_2})$ for any pair $\{\tau_1, \tau_2\}$ is small compared to the KLD computed between a pair of scaled histograms for which τ is outside the scaling region.

The scaled KL divergence histograms for a subset of 6 years are shown in Fig. 5. The baseline histogram comprised of KL divergences computed for $\{\tau_1, \tau_2\}$ outside the scaling regime ($\tau < 1000$) is in red. We ensure that the number of samples contributing to each histogram are comparable. The histogram corresponding to the scaling regime ($1000 \leq \tau \leq 30000$) has a lower mean KLD compared to the baseline. This suggests that the shape of $\tilde{p}_\tau(\cdot)$ is more stable *within* the scaling regime rather than outside it.

- **Probing the onset of the scaling regime using Gaussian Mixture Models and Kurtosis:** We fit a Gaussian Mixture Model (GMM) (2-mode) on $\tilde{p}_\tau(\cdot)$ and probe the weights of the two components across τ . We expect to see a transition as the scaling regime sets in. In Fig. 6, observe that while before the scaling regime sets in one mode is dominant. And as the scaling starts at $\tau = 1000$, the weights of the two modes become comparable (mode 1 corresponds to the mode with the lower standard deviation). We observe this pattern with 3, 4, 5 mode fits as well.
- **Kurtosis of the density function with respect to τ :** In Fig. 7, we demonstrate the transition into the scaling regime by plotting the kurtosis of $\tilde{p}_\tau(\cdot)$ with respect to τ . When the scaling property takes effect, the kurtosis values suggest a corresponding transition of $\tilde{p}_\tau(\cdot)$ from leptokurtic (> 3) to platykurtic (< 3) regimes.

IV. GENERATIVE MODELS

We have observed so far that real S&P500 data demonstrates (a) variable MST structures that represent stock interactions, and more specifically vine-like structures that represent the different sectors for larger values of τ ; and (b) an empirical scaling law governing the inverse standard deviations of histograms of market-mode adjusted correlations – both dependent on τ . Additionally we have shown that during the scaling regime, the functional form of the scaled distribution remains relatively stable. Next, we consider the task of formulating stochastic models for the returns time series. As we will see, common generative models used in financial modeling – such as the single- and multi-factor models do not replicate these behaviors. We propose an alternate that is more promising.



FIG. 5. The histogram of pairwise KL divergences inside and outside the scaling regime over 6 years of analysis. The histogram corresponding to scaling (in blue) is left-shifted compared to the baseline (in red) suggesting that the functional form in the scaling regime is more stable than outside it.

A. Factor models

1. Single Factor Model

The conventional single-factor model [22] uses only the fluctuations of the market mode and individual stock prices to model the correlations of return, i.e.,

$$r_i(t) = \alpha_i + \beta_i r_0(t) + \xi_i(t), \quad (\text{IV.1.1})$$

where $r_0(t)$ represents the market mode describing the overall fluctuation of the financial market. In Eq. (IV.1.1), $\xi_i(t)$ is the part not included in the market mode. In the one-factor model, $\xi_i(t)$ is a zero mean Gaussian distributed time series with $\langle \xi_i^2 \rangle = \epsilon_i^2$ and is independent of each other and $r_0(t)$. In fact, we can derive the values of the correlation coefficients in the one-factor model: $\rho_{ij} = \rho_{i0}\rho_{j0}$. Thus, the residuals $\{c_{i,j}(\tau)\}_{i,j=1}^N = 0$ in Eq. (II.1.9). The scaled distribution $\tilde{p}_\tau(\cdot)$ in Eq. (II.2.2) trivially becomes the delta function ($\mu = 0$, $b(\tau) \rightarrow \infty$). Clearly, the single-factor model is not consistent with data.

2. Multi-Factor Model

The MSTs of the pairwise stock correlations clearly show clustering of stocks belonging to the same sector, and hence one can formulate a multi-factor model, where additional parameters corresponding to sectors are incorporated. Since the computational models we are considering directly simulate returns (not the prices), one needs to introduce an additional parameter to simulate the effect of time scale τ : by varying this parameter, one can control whether the market mode dominates –drowning out the effect of the sectors (as observed for small τ in real data)– or the market mode’s effect is attenuated allowing the sector correlations to emerge (as observed for large τ).

Consider K sectors in a market. The multi-factor model takes the form:

$$r_i(t; \tilde{\eta}) = \tilde{\alpha}_i + \tilde{\beta}_i r^{\text{mar}}(t) + \sum_{k=1}^K \tilde{\gamma}_{i,k} r_k^{\text{sec}}(t) + \tilde{\xi}_i(t; \tilde{\eta}), \quad (\text{IV.1.2})$$

where,

$$r^{\text{mar}}(t + \Delta t) - r^{\text{mar}}(t) \sim \mathcal{N}(0, 0.050 \times \Delta t), \quad (\text{IV.1.3})$$

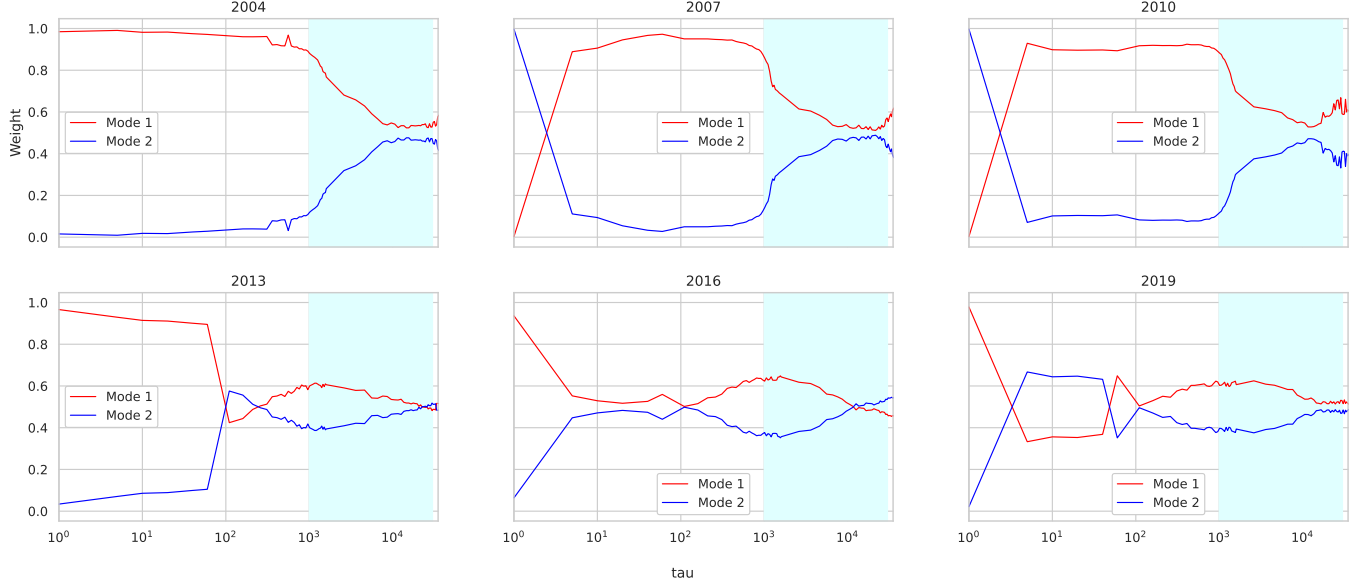
Probing GMM weights as a measure-of-fit for f across different taus

FIG. 6. Capturing the scaling regime onset by fitting 2-mode GMM onto the scaled correlation histograms. Across 6 years of analysis, we plot the weights of the 2 GMM components after fitting to $\tilde{p}_\tau(\cdot)$ for different τ . As τ is increased, the second mode starts contributing significantly to the fit signaling the onset of the scaling regime (shaded cyan).

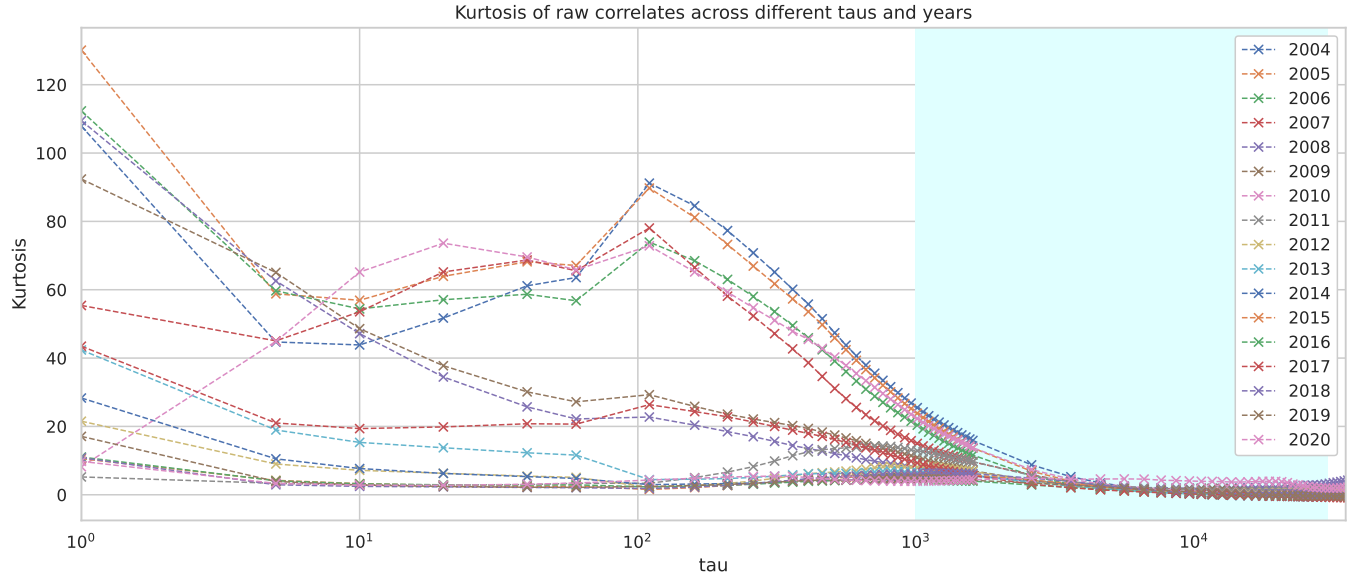


FIG. 7. Leptokurtic-to-platykurtic kurtoses transition in the correlation histograms as the scaling (shaded cyan) takes effect. The higher values of kurtosis for smaller τ indicate sharper peaks in the correlation histograms (compared to a normal distribution) that can in fact be visually verified in Fig. 4 (leptokurtic regime). As τ increases, the correlation distribution becomes more flat resulting in lower kurtosis (platykurtic regime).

$$r^{\text{sec}}(t + \Delta t) - r^{\text{sec}}(t) \sim \mathcal{N}(0, 0.10 \times \Delta t), \quad (\text{IV.1.4})$$

and, for $i = 1, 2, \dots, N$,

$$\tilde{\xi}_i(t; \tilde{\eta}) := \frac{d}{dt} \tilde{\Xi}_i(t, \cdot), \quad (\text{IV.1.5})$$

$$\tilde{\Xi}_i(t + \Delta t, t) := \mathcal{N}(0, \tilde{\eta}^2 \times \Delta t). \quad (\text{IV.1.6})$$

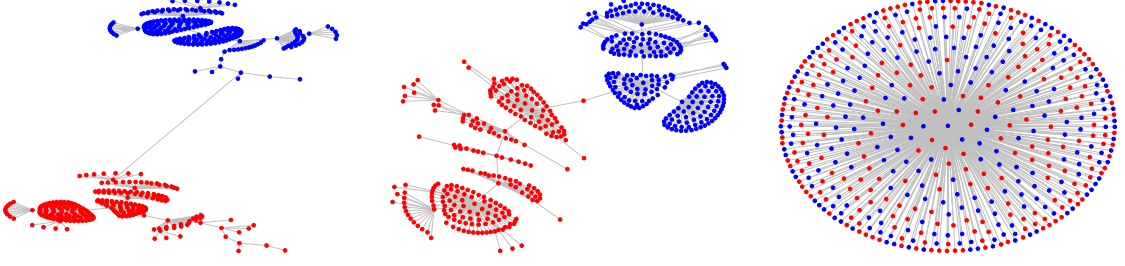


FIG. 8. MSTs of the multi-factor models. The sector for each stock (node) is indicated by its color. We varied $\tilde{\eta}$: (left) $\tilde{\eta} = 0.1$, (center) $\tilde{\eta} = 10.0$, and (right) $\tilde{\eta} = 1000.0$. We set the number of steps 10000 and $\mu_{\tilde{\gamma}} = 1.0$. Observe for small $\tilde{\eta}$, the sectors are separated into distinct groups in the MST – similar to when τ is large. As $\tilde{\eta}$ increases, the groups lose identity and merge; i.e the sector information is devalued: a similar effect to when τ is small. Precision in the edge weights is set to 1.

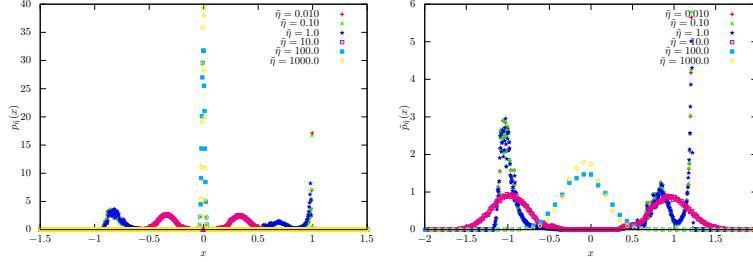


FIG. 9. (a) Histogram $p_{\tilde{\eta}}(x)$ in Eq. (II.2.1) of the multi-factor model; (b) Scaled histogram $\tilde{p}_{\tilde{\eta}}(x)$ in Eq. (II.2.2). We set the number of steps 10000 and $\mu_{\tilde{\gamma}} = 1.0$.

Here, $\mathcal{N}(\mu, \sigma^2)$ is the Gaussian perturbation function and $\tilde{\gamma}_{i,k}$ is non-zero when stock i belongs to sector k and 0 otherwise. Additionally, the variance for market and sector returns ($0.05 \times \Delta t, 0.10 \times \Delta t$) match the relative volatility observed in real-data. Note that increasing $\tilde{\eta}$ corresponds to larger perturbations of $\tilde{\xi}_i(t)$ in successive time steps. Thus it plays the role of $1/\tau$: a large $\tilde{\eta}$ implies market-mode dominance and small $\tilde{\eta}$, sector-mode dominance (see Figs. 8 and 9).

We performed the numerical simulation of the multi-factor model with $K = 2$ sectors. We set $N = 500$ and the number of stocks in each sector as 250. We swept $\tilde{\eta}$ in Eq. (IV.1.6) across multiple values. The other parameters are set to [23]: $\tilde{\alpha}_i \sim \mathcal{N}(0.0, 1.0)$, $\tilde{\beta}_i \sim \mathcal{N}(0.0, 1.0)$, and $\tilde{\gamma}_{i,k} \sim \mathcal{N}(\mu_{\tilde{\gamma}}, 1.0)$ if stock i belongs to sector k and otherwise zero. In Fig. 8, we show the MSTs of the multi-factor models for $\tilde{\eta} = 0.1, 10.0, 1000.0$ and $\mu_{\tilde{\gamma}} = 1.0$. Observe that for small $\tilde{\eta}$, the stocks per sector belong in separate communities in the MST. As $\tilde{\eta}$ increases, the communities collapse.

In Fig. 9, we plot the histogram $p_{\tilde{\eta}}(\cdot)$ in Eq. (II.2.1) of the multi-factor model and scaled histogram $\tilde{p}_{\tilde{\eta}}(\cdot)$ in Eq. (II.2.2) (see SM Section S-II for histograms generated using an exhaustive set of combinations of $\tilde{\eta}$ and $\mu_{\tilde{\gamma}}$). The following dynamics are observed: (a) For small $\tilde{\eta}$ – may correspond to large τ – two peaks originate from two sector modes and one peak originates from the market mode; (b) for moderate $\tilde{\eta}$, the market mode dissipates and the two sector modes dominate the distribution; and (c) for large $\tilde{\eta}$, the return correlation distribution becomes random due to large perturbations. The multi-factor model explicitly uses sector affiliation as a parameter resulting in multi-modal correlation distributions - a property not consistent with the empirical evidence. Additionally, this multi-modal structure of $\tilde{p}_{\tilde{\eta}}(\cdot)$ implies $b(\tau)$ does not scale with τ .

B. Modified Vicsek model

The Vicsek model is a generative model that can display some of the salient group characteristics of swarming behavior, as observed in the motion patterns of flocks of birds and swarms of fish. Compared to the multi-factor model where group assignments are provided in advance, such assignments emerge naturally in the Vicsek model: each particle in the swarm is influenced by other particles that are within a neighborhood. Based on such local-only interactions, long distance order emerges and groups of particles cluster together in their dynamical behavior, akin to sectors emerging in stock markets.

Our model uses the standard setup [24] with the following modifications (see SM Section S-IV for a derivation):

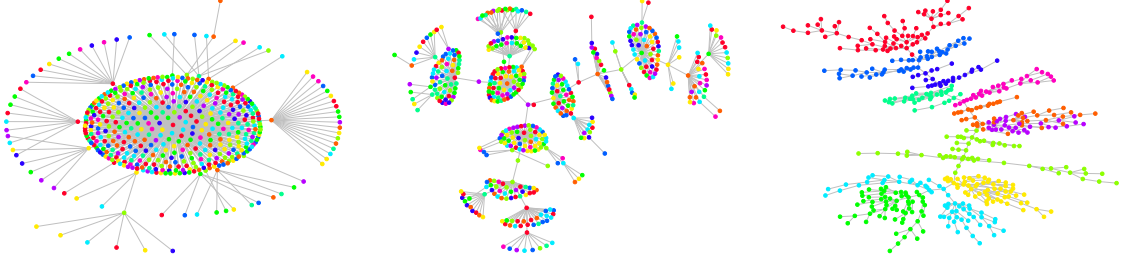


FIG. 10. MSTs rendered using the modified Vicsek generative model. We varied η : (a) $\eta = 0.010$ (b) $\eta = 1.0$ (c) $\eta = 100.0$. We set the number of steps 10000 and $\delta = 0.10$. 11 communities – equal to the number of GICS sectors – are identified in the MST with $\eta = 100.0$ and the stocks associated to each sector are tracked as η decreases for the fixed δ [25]. Observe that the sectors collapse for low η : as η decreases, the fixed neighborhood of δ encourages more particles (stocks) to interact with one since they are perturbed to a lesser extent by Ξ . This leads to homogeneous behavior and the radial MSTs.

(a) Consistent with the factor model setup the predicted variable is the return $r_i(t)$; (b) Particles (individual stocks) move in \mathbb{R}^1 (rather than in \mathbb{R}^2); a stock's offset from 0 is the return value. The proximity of one particle i to another j at time t is the absolute value of the difference of the returns $|r_i(t) - r_j(t)|$ rather than the typical cosine distance metric used in \mathbb{R}^2 ; (c) Time steps are discretized rather than continuous. The update step is:

$$\begin{aligned} \alpha_i r_i(t + \Delta t) &= (\alpha_i - \beta_i \Delta t) r_i(t) \\ &+ \frac{\gamma_i}{N_{i,\delta}} \sum_{j: |r_i(t) - r_j(t)| < \delta} (r_j(t) - r_j(t - \Delta t)) \\ &+ \Xi_i(t + \Delta t, t), \end{aligned} \quad (\text{IV.2.1})$$

where

$$\Xi_i(t + \Delta t, t) \sim \mathcal{N}(0.0, \eta^2 \Delta t), \quad (\text{IV.2.2})$$

and $N_{i,\delta}$ is the number of elements j that satisfy $|r_i(t) - r_j(t)| < \delta$. Increasing η corresponds to large perturbations of $r_i(t)$ (similar to the role played by $\tilde{\eta}$ in the multi-factor model). δ is the distance within which one particle can influence another and may corresponds to the effect of τ . When δ is very small, particles move mostly independently of one another. Indeed, in many ways, δ and η behave as duals of one another. As δ increases, groups of particles move together as swarms, a model for stock market sectors. We set $N = 500$, $\alpha_i = \gamma_i = 1.0$ and $\beta_i = 0.05$ for $i = 1, 2, \dots, N$, and $\Delta t = 1.0$. The evaluation is similar to that of the factor models (additional correlation histograms computed using several combinations of η and δ are presented in SM Section S-III):

- *Structure of the MST:* In Fig. 10, we observe that by increasing η the MST structure transitions from radial to the vine-like structure observed empirically: a result of smaller communities of particles being formed due to the large noise term perturbing particles to deviate from within a δ radius of influence.
- *Functional form of the correlation histograms:* In Figs. 11 and 12, we plot the correlation histogram $p_{(\cdot)}(\cdot)$ and its scaled form $\tilde{p}_{(\cdot)}(\cdot)$ by sweeping η for a fixed δ and sweeping δ for a fixed η . Observe that the shape of the correlation histogram and scaled correlation histogram varies as a function of η and δ , qualitatively similar to the effect induced by sweeping $1/\tau$ and τ for the scaling law in the original stock market data (see Figs. 3 and 4 for a comparison with the empirical visual evidence).
- *Scaling behavior with respect to η and δ :* In Fig. 13, we plot the scaling laws for the Vicsek model: $b(\cdot)$ w.r.t η and δ (compare to Fig. 2). The scaling trend is divided into three distinct phases: (a) For small η or large δ , particles (stocks) oscillate in synchronization because the interaction term dominates the system. (b) As η is increased or δ is decreased, particles are encouraged to move in smaller groups during which the scaling effect is observed. (c) For very large η or very small δ , the noise term simply dominates the dynamics, zeroing the correlations between particles.

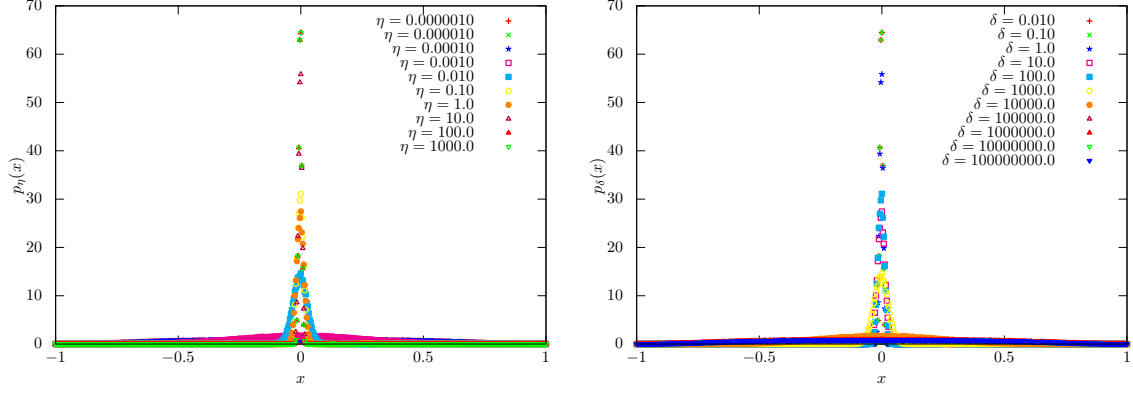


FIG. 11. (a) Histogram $p_\eta(x)$ in Eq. (II.2.1) generated using the modified Vicsek model. Note that the subscript is changed from τ to η . We set $\delta = 1.0$ and the number of steps 10000. (b) Histogram $p_\delta(x)$ in Eq. (II.2.1) from the modified Vicsek model. Note that the subscript is changed from τ to δ . We set $\eta = 10.0$ and the number of steps 10000. Histograms with other choices of η and δ are provided in SM Section S-IV.

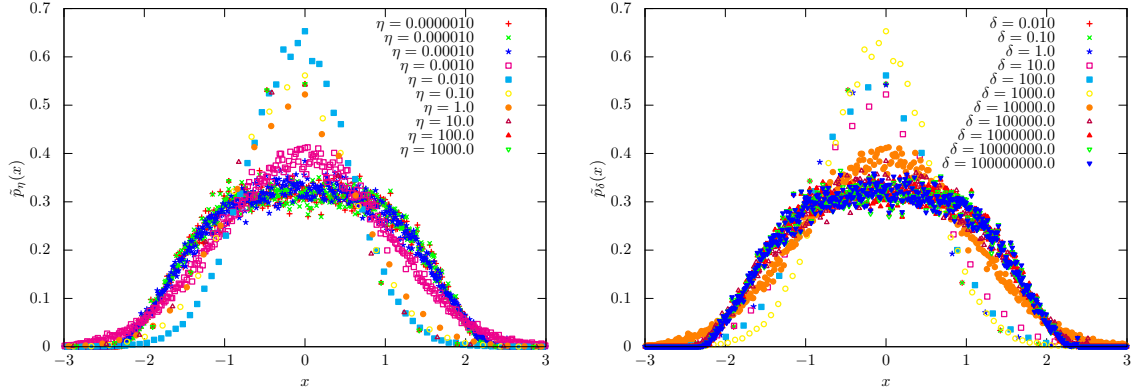


FIG. 12. (a) Scaled histogram $\tilde{p}_\eta(x)$ in Eq. (II.2.2) of the modified Vicsek model. Note that the subscript is changed from τ to η . We set $\delta = 1.0$ and the number of steps 10000. (b) Scaled histogram $\tilde{p}_\delta(x)$ in Eq. (II.2.2) of the modified Vicsek model. Note that the subscript is changed from τ to δ . We set $\eta = 10.0$ and the number of steps 10000.

V. CONCLUDING REMARKS

In this paper, we demonstrate a robust scaling law with respect to τ – the time gap used to compute stock price return – that governs the inverse standard deviation $b(\tau)$ of the histogram of market-mode adjusted correlations of returns $p_\tau(\cdot)$. We additionally observe that during the scaling regime, the functional form of the scaled versions of the histograms $\tilde{p}_\tau(\cdot)$ remains relatively stable. Finally we review existing stochastic and generative factor models to show that they do not model the emergent phenomena and propose a modified Vicsek model that is a more promising candidate. The scaling law was demonstrated yearly from 2004 to 2020 on real stock price data sampled every minute of trading hours.

The evidence of the robust scaling law motivates investigating whether the scaling exponent λ is a macro-economic indicator of market health. In Fig. 14(a), λ is plotted w.r.t year using different timescales $T_{int} = 1$ month, 3 months, 6 months, and 12 months. From 2004 to 2020, the absolute value gradually decreases. In fact, the rising values of λ can be linked to increased market volatility: when $|\lambda| \rightarrow 0$, $b(\tau) \rightarrow 1$ ($b(\tau) \leq 1$ for $\tau \geq 1$) is independent of τ . Therefore, the standard deviations $1/b(\tau)$ are small and also independent of τ : i.e most pair-wise return correlations are close to 0 and so, the return sequences are noisy irrespective of whether a given investor is looking to invest in the short-term or the long-term - a key indicator of *market volatility*. Indeed, the anomalous values of λ in 2008 and 2020 are likely due to the subprime mortgage crisis and the COVID-19 pandemic.

In summary, the discovery of such emergent phenomena as the scaling law and its associated summary statistics in the correlations of stock price returns adds to a growing body of work in macro-economic modeling. By extending the qualitative observations of the variations in MST structure to the correlations at large in a quantifiable manner, we

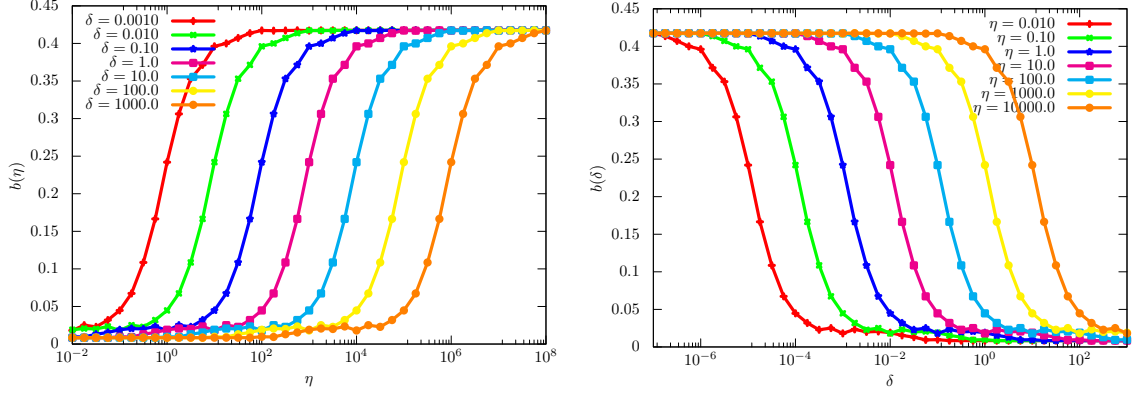


FIG. 13. (a) The relationship between η in the modified Vicsek model and $b(\eta)$, which is the scale factor. Note that we changed the argument from τ to η . We set the number of steps 10000. (b) The relationship between δ in the modified Vicsek model and $b(\delta)$, which is the scale factor. Note that we changed the argument from τ to δ . We set the number of steps 10000.

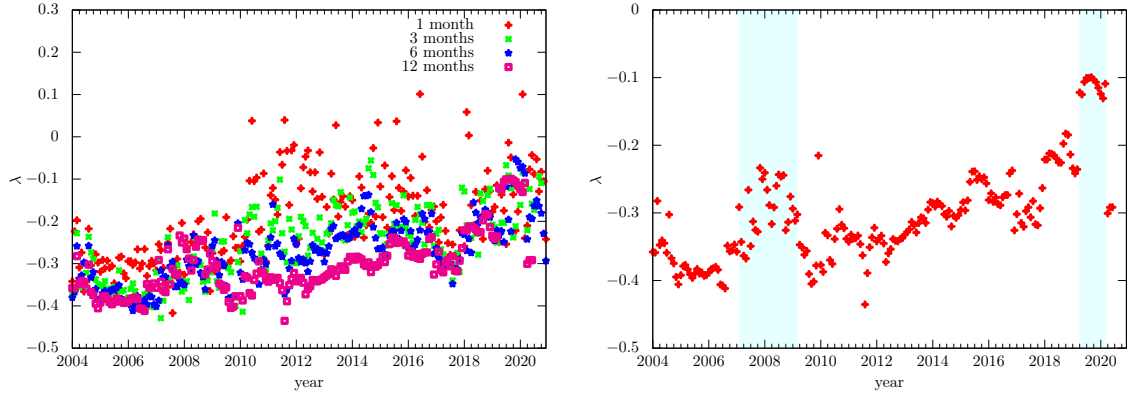


FIG. 14. (a) Values of λ from 2004 to 2020 with the intervals of 1 month, 3 months, 6 months, and 12 months. (b) Values of λ from 2004 to 2020 with interval 1 year. The definition of λ is given in Eq. (II.2.3). In the blue highlighted regimes, anomalies are observed. This may correspond to the increased market volatility in those years: the subprime mortgage crisis, the bankruptcy of Lehman Brothers in 2007/2008 and the COVID-19 pandemic in 2019/2020.

demonstrate one robust path to probe market health that is a promising alternative to directly modeling individual agents, who are often unpredictable in their financial decision-making, and who oftentimes behave as irrational agents while deciding investment strategy.

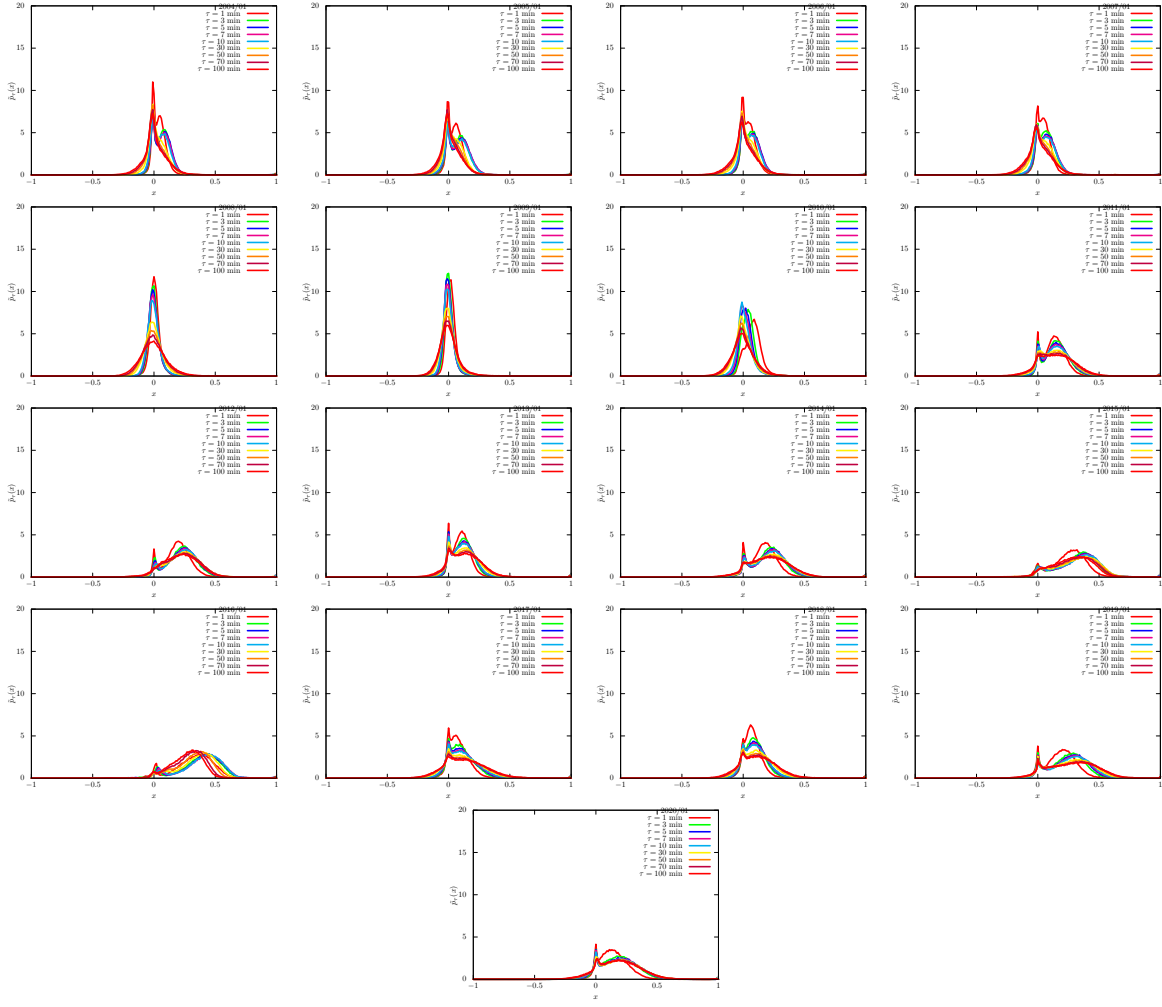


FIG. 15. Histogram $p_\tau(\cdot)$ in Eq. (II.2.1). We set T_{int} 1 month.

Appendix A: Additional numerical simulations using real-data

In Fig. 2, we observed a dependence of the scaling factor $b(\tau)$ on τ when the total investment duration $T_{\text{int}} = 1$ year. In this section, we demonstrate similar characteristics and small variations in the robustness of scaling by varying T_{int} .

1. When T_{int} is 1 month

In Fig. 15, we show $p_\tau(\cdot)$ in Eq. (II.2.1) for small τ and $T_{\text{int}} = 1$ month (January) from 2004 to 2020. Fig. 16 plots $p_\tau(\cdot)$ with respect to large τ where for each year. Figs. 17, 18 shows the scaled distribution $\tilde{p}_\tau(\cdot)$ for small and large τ . In Fig. 19, we plot the dependence of the scaling factor $b(\tau)$ on τ from 2004 to 2020. In each of these plots, there are 12 trend lines of $b(\tau)$ w.r.t τ such that each line corresponds to 1 month of analysis: i.e $T_{\text{int}} = 1$ month and we vary the starting time point t_{ini} from January 1st to December 1st with a stride of 1 month. In Fig. 20, we plot the line estimating the power law function during the scaling regime for the samples $\tau, b(\tau)$ from 2004 to 2020. Finally, in Fig. 21, we plot the values of λ , which is the scaling exponent given in Eq. (II.2.3).

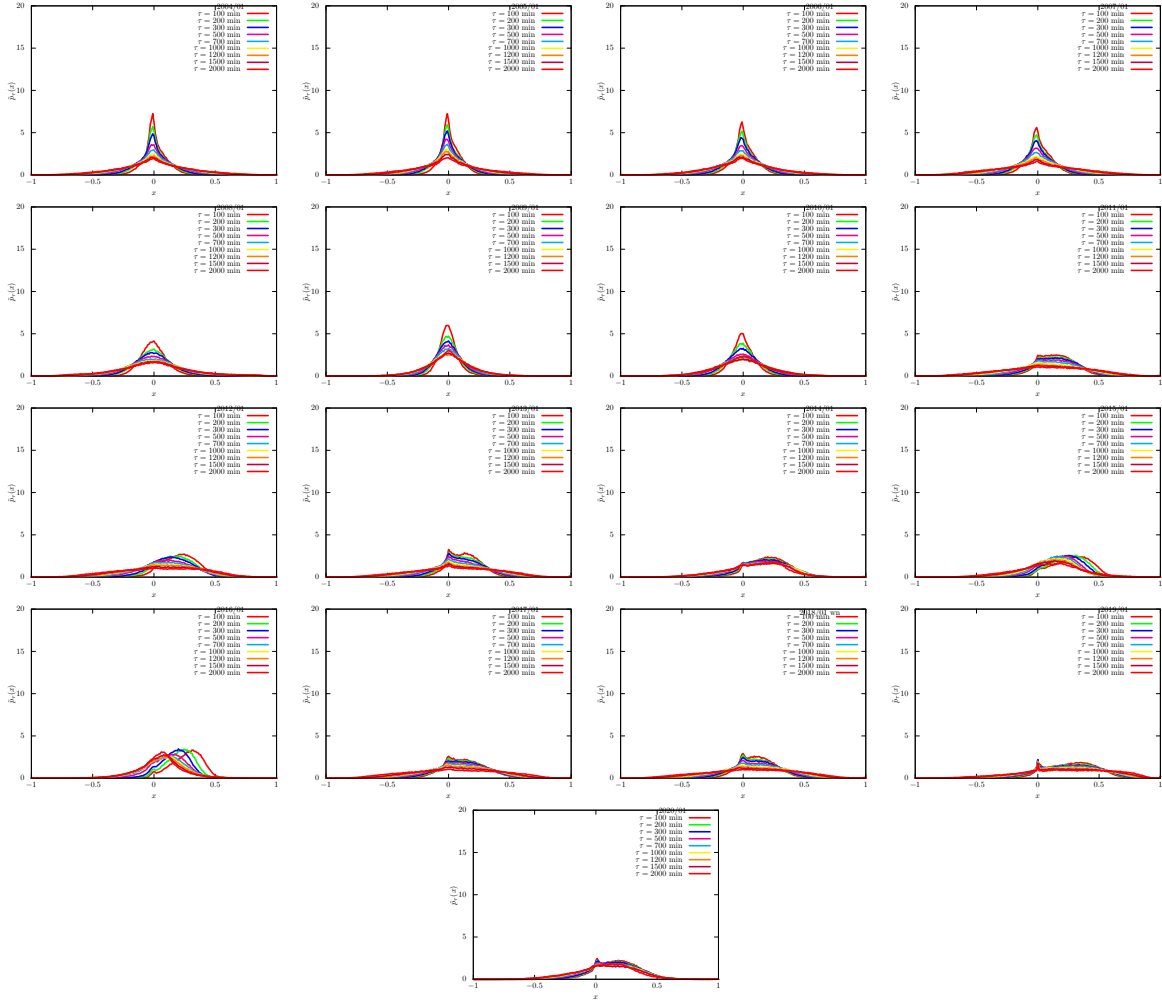


FIG. 16. Histogram $p_\tau(\cdot)$ in Eq. (II.2.1). We set T_{int} 1 month.

2. When T_{int} is 3 months

Fig. 22 plots $p_\tau(\cdot)$ with respect to small τ and Fig. 23 for large τ . Figs. 24, 25 shows the scaled distribution $\tilde{p}_\tau(\cdot)$ for small and large τ . In Fig. 26, we plot the dependence of the scaling factor $b(\tau)$ on τ from 2004 to 2020. In each of these plots, there are 12 trend lines of $b(\tau)$ w.r.t τ such that each line corresponds to 3 months of analysis: i.e $T_{\text{int}} = 3$ months and we vary the starting time point t_{ini} from January 1st to December 1st with a stride of 1 month. Note: the last window in this evaluation is December 1st to Feb 27/28 of the next year. In Fig. 27, we plot the line estimating the power law function during the scaling regime for the samples $\tau, b(\tau)$ from 2004 to 2020. Finally, in Fig. 28, we plot the values of λ .

3. When T_{int} is 6 months

Figs. 29, 30 plot $p_\tau(\cdot)$ with respect to small and large τ respectively. Figs. 31, 32 shows the scaled distribution $\tilde{p}_\tau(\cdot)$ for small and large τ . In Fig. 33, we plot the dependence of the scaling factor $b(\tau)$ on τ from 2004 to 2020. In each of these plots, there are 12 trend lines of $b(\tau)$ w.r.t τ such that each line corresponds to 1 month of analysis: i.e $T_{\text{int}} = 6$ months and we vary the starting time point t_{ini} from January 1st to December 1st with a stride of 1 month. In Fig. 34, we plot the line estimating the power law function during the scaling regime for the samples $\tau, b(\tau)$ from 2004 to 2020. Finally, in Fig. 35, we plot the values of λ .

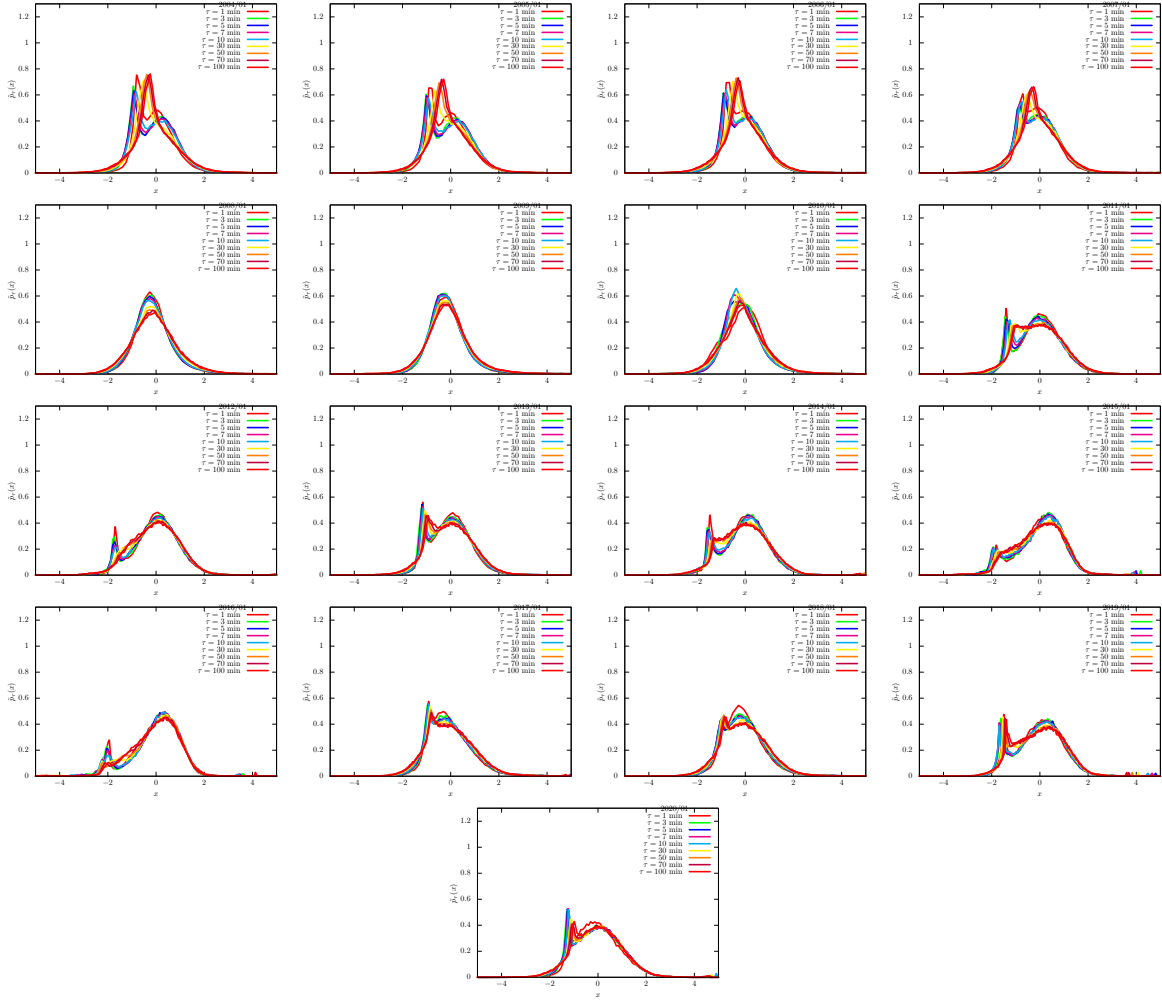


FIG. 17. Scaled histogram $\tilde{p}_\tau(\cdot)$ in Eq. (II.2.2). We set T_{int} 1 month.

4. When T_{int} is 12 months

Fig. 36 plots $p_\tau(\cdot)$ with respect to small τ and Fig. 37 for large τ . Figs. 38, 39 shows the scaled distribution $\tilde{p}_\tau(\cdot)$ for small and large τ . In Fig. 40, we plot the dependence of the scaling factor $b(\tau)$ on τ from 2004 to 2020. In each of these plots, there are 12 trend lines of $b(\tau)$ w.r.t τ such that each line corresponds to 1 month of analysis: i.e $T_{\text{int}} = 12$ months and we vary the starting time point t_{ini} from January 1st to December 1st with a stride of 1 month. In Fig. 41, we plot the line estimating the power law function during the scaling regime for the samples $\tau, b(\tau)$ from 2004 to 2020. Finally, in Fig. 42, we plot the values of λ .

5. Scaling exponents

In Fig. 43, we plot the combined plots of the values of λ with respect to year (with the intervals of 1 month, 3 months, 6 months, and 12 months).

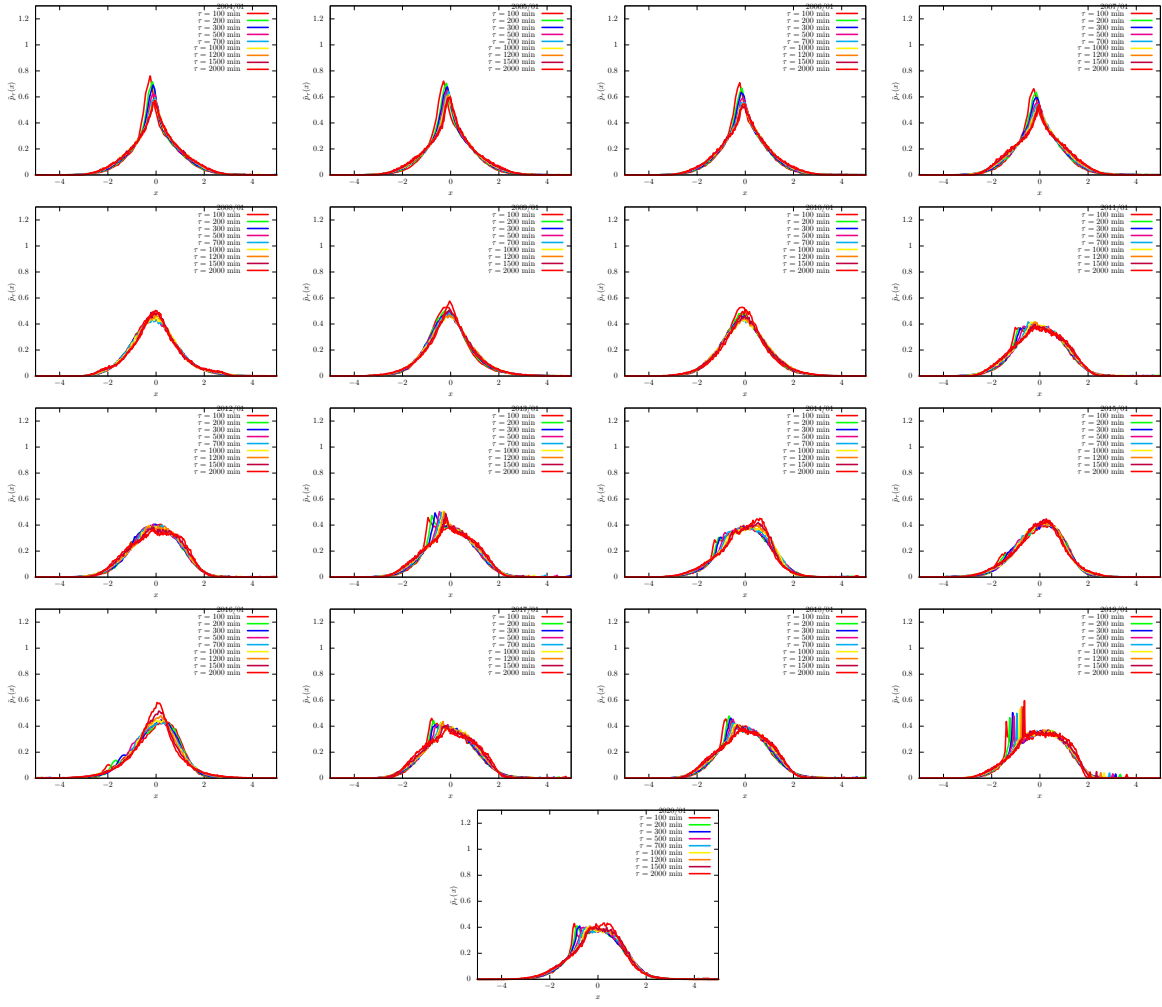


FIG. 18. Scaled histogram $\tilde{p}_\tau(\cdot)$ in Eq. (II.2.2). We set T_{int} 1 month.

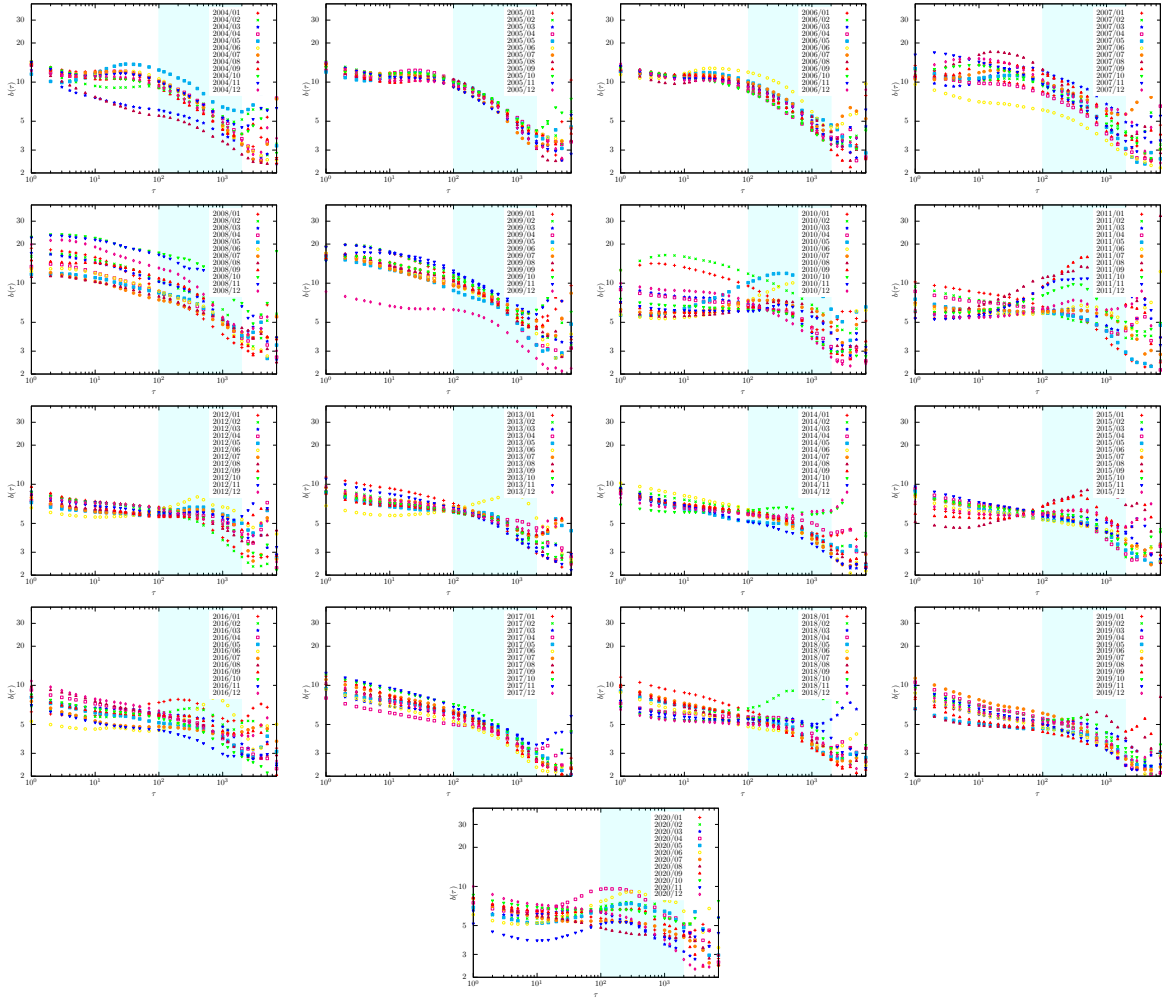


FIG. 19. Dependence of the scaling factor $b(\tau)$ on τ from 2004 to 2020. We set T_{int} 1 month and varied t_{ini} from January 2004 to December 2020 by a month.

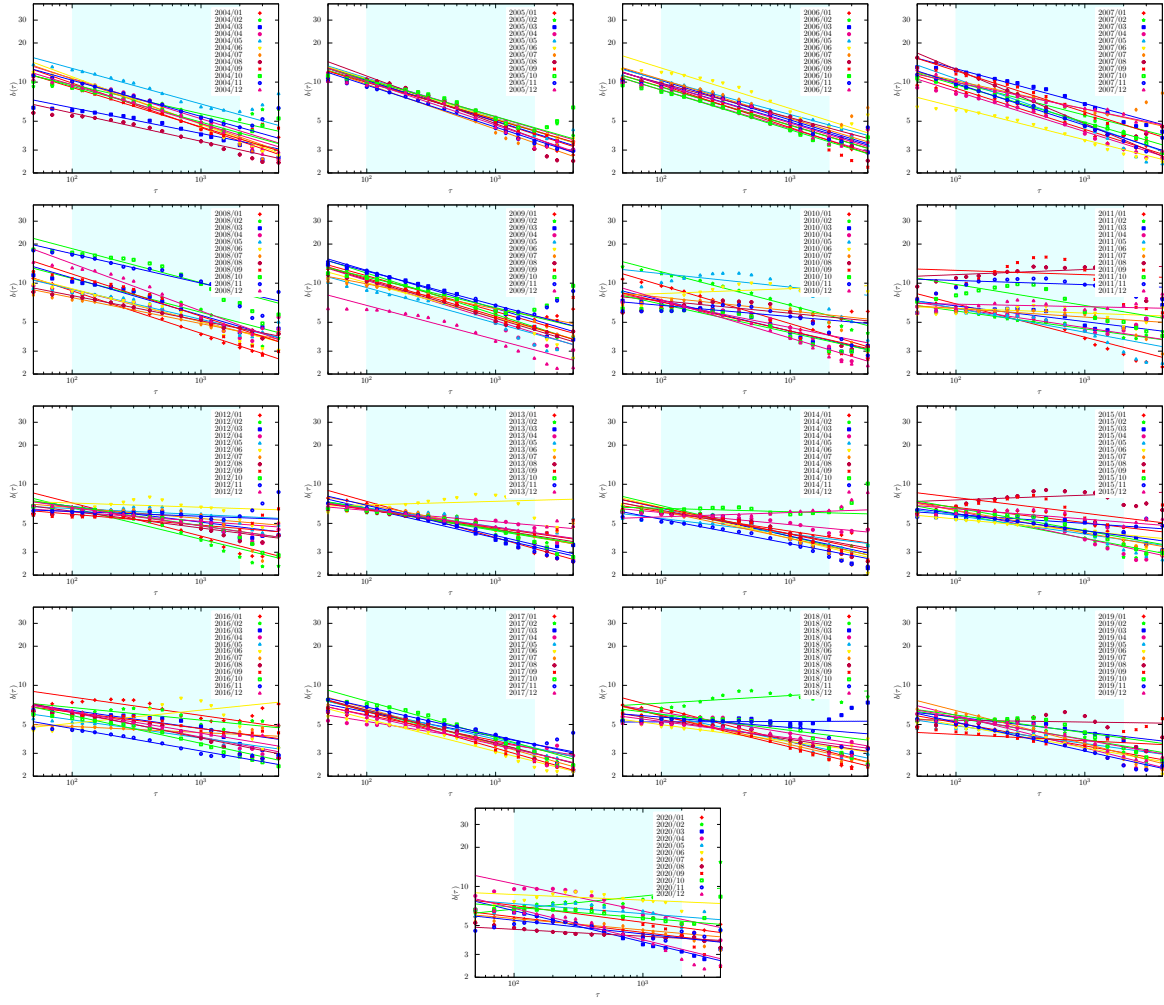


FIG. 20. Trendlines highlighting the range of τ during which the scaling phenomena is observed from 2004 to 2020. We set T_{int} 1 month and varied t_{ini} from January 2004 to December 2020 by a month.

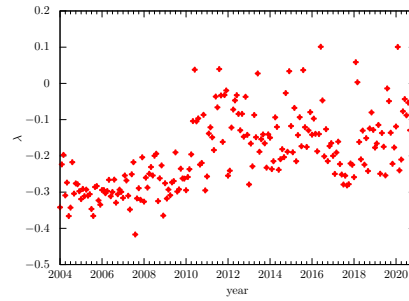


FIG. 21. Values of λ from 2004 to 2020 when the interval is 1 month.

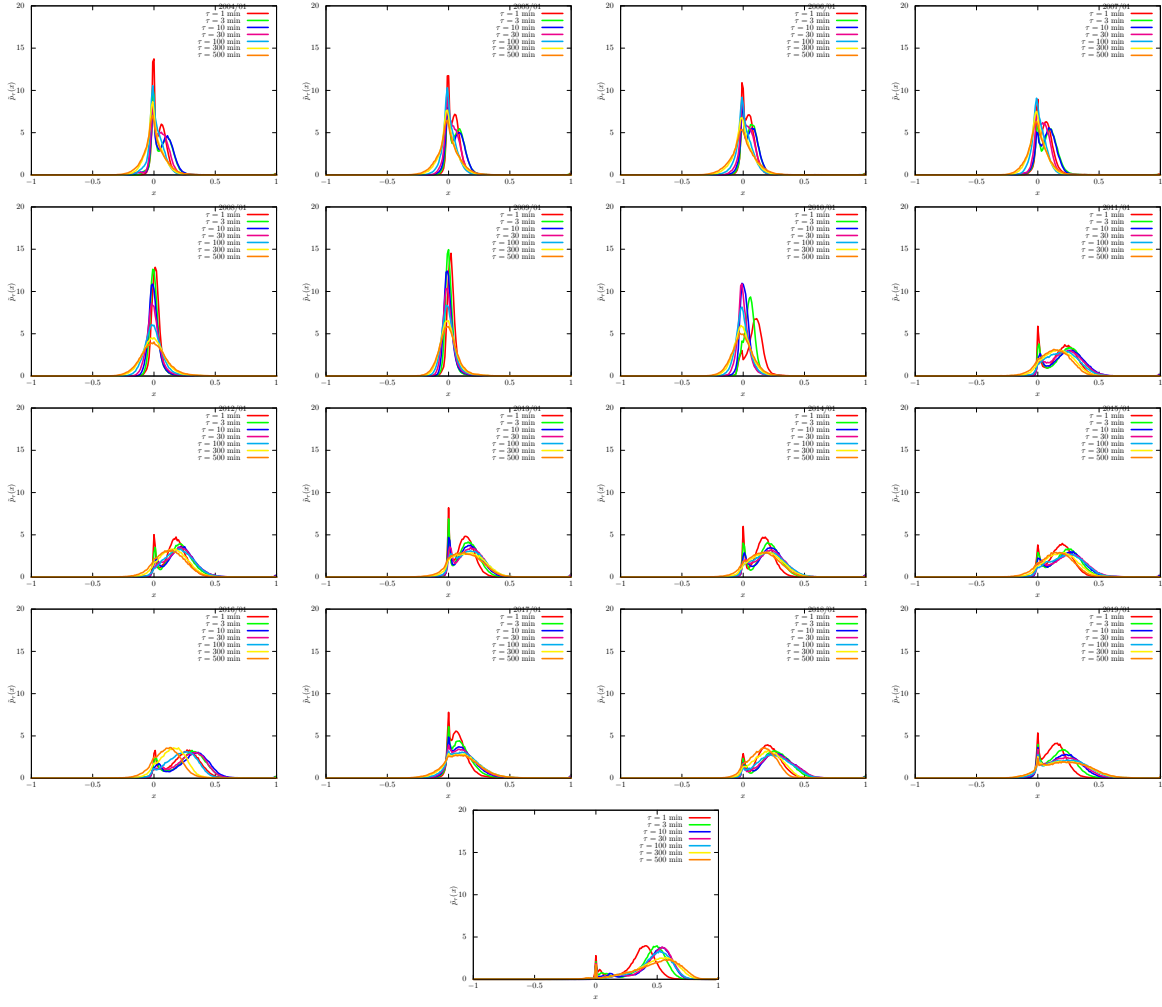


FIG. 22. Histogram $p_\tau(\cdot)$ in Eq. (II.2.1). We set T_{int} 3 months.

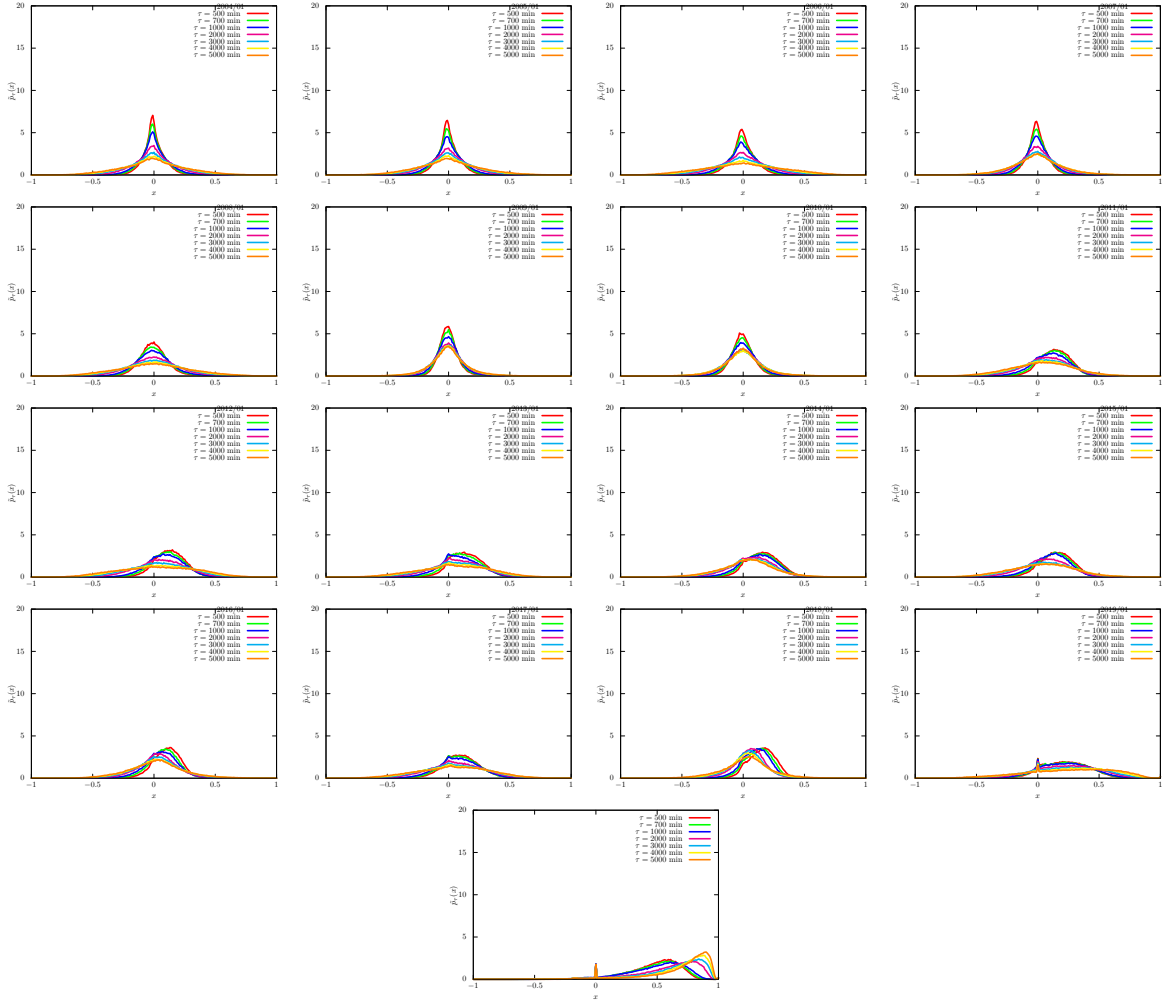


FIG. 23. Histogram $p_\tau(\cdot)$ in Eq. (II.2.1). We set T_{int} 3 months

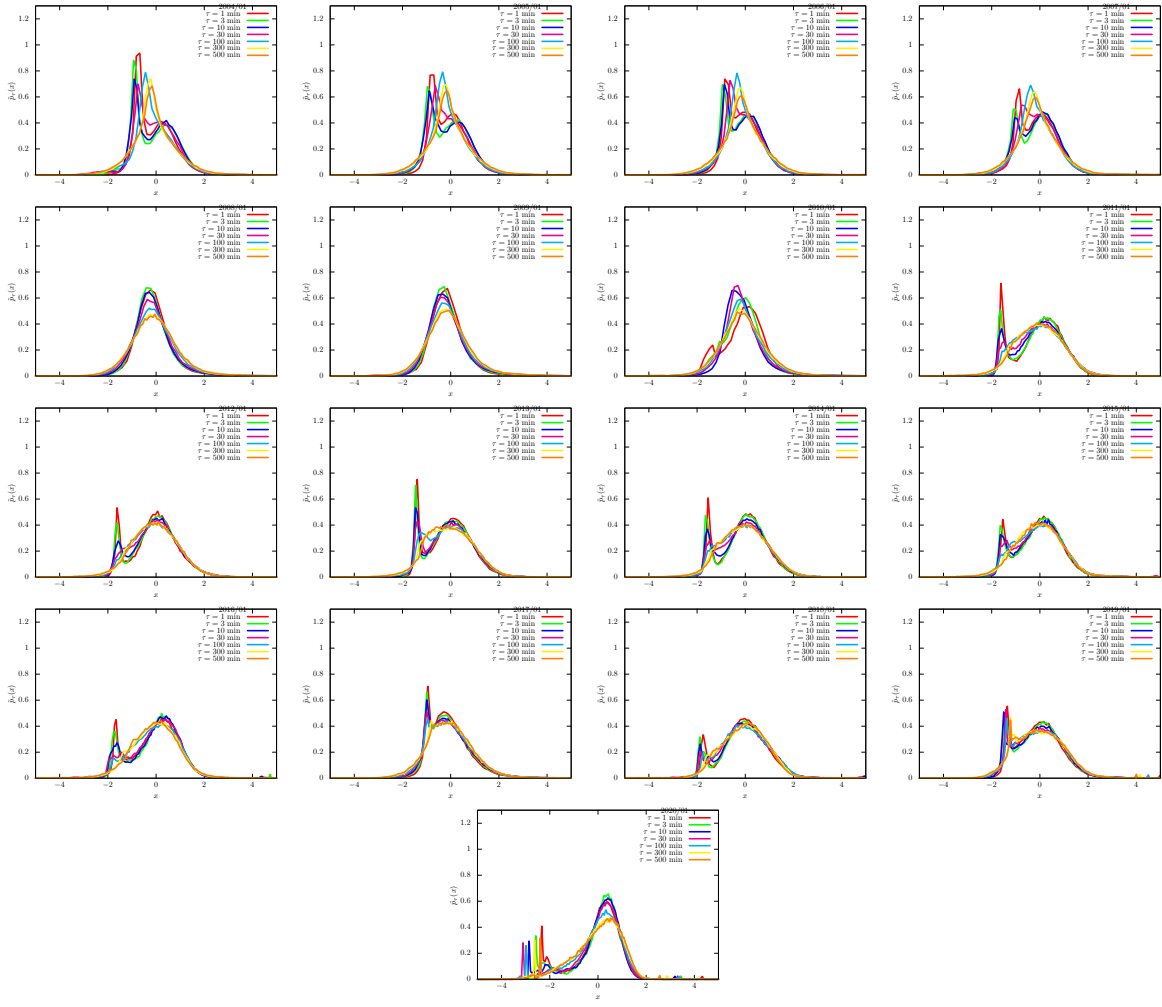


FIG. 24. Scaled histogram $\tilde{p}_\tau(\cdot)$ in Eq. (II.2.2). We set T_{int} 3 months.

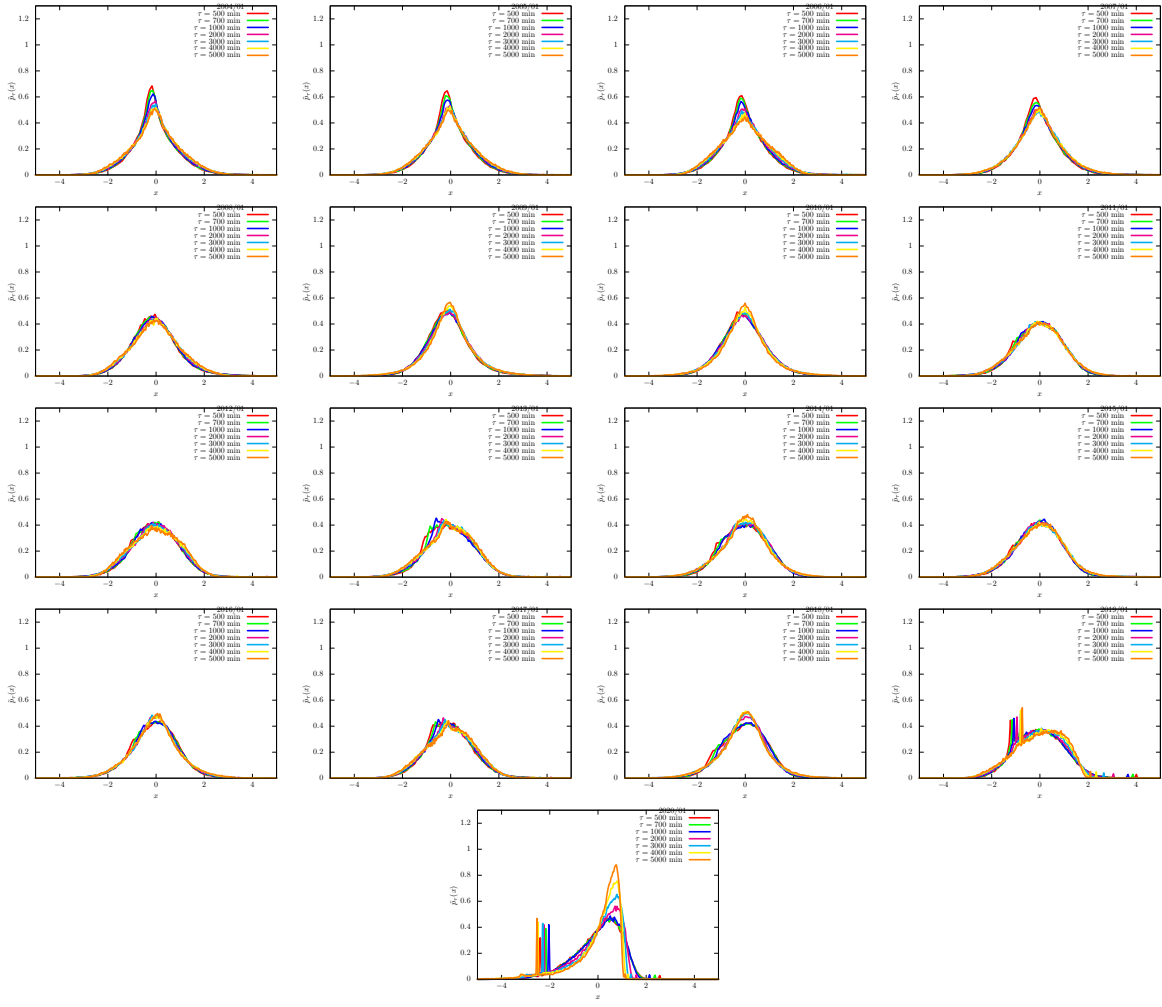


FIG. 25. Scaled histogram $\tilde{p}_\tau(\cdot)$ in Eq. (II.2.2). We set T_{int} 3 months.

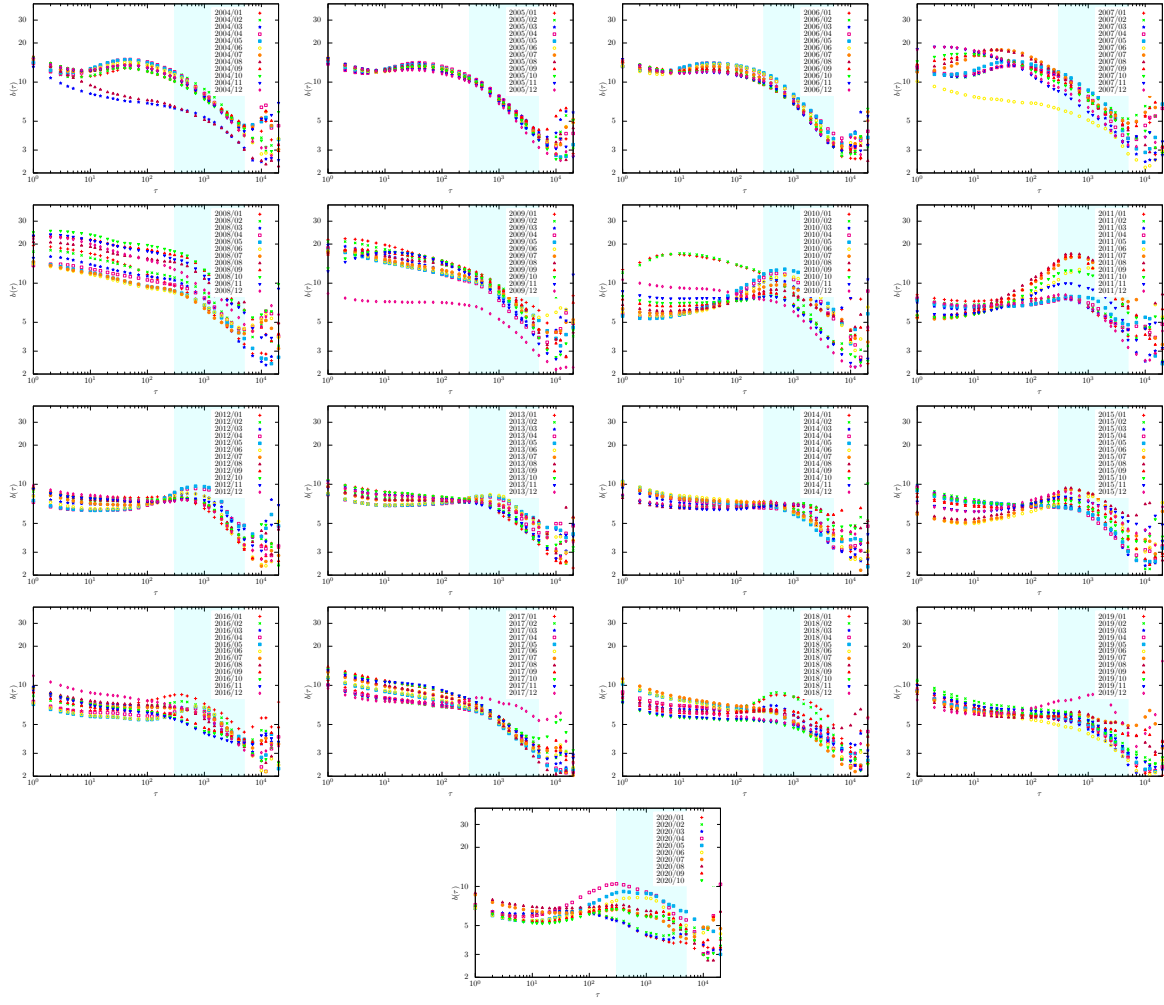


FIG. 26. Dependence of the scaling factor $b(\tau)$ on τ from 2004 to 2020. We set T_{int} 3 months and varied t_{ini} from January 2004 to December 2020 by a month.

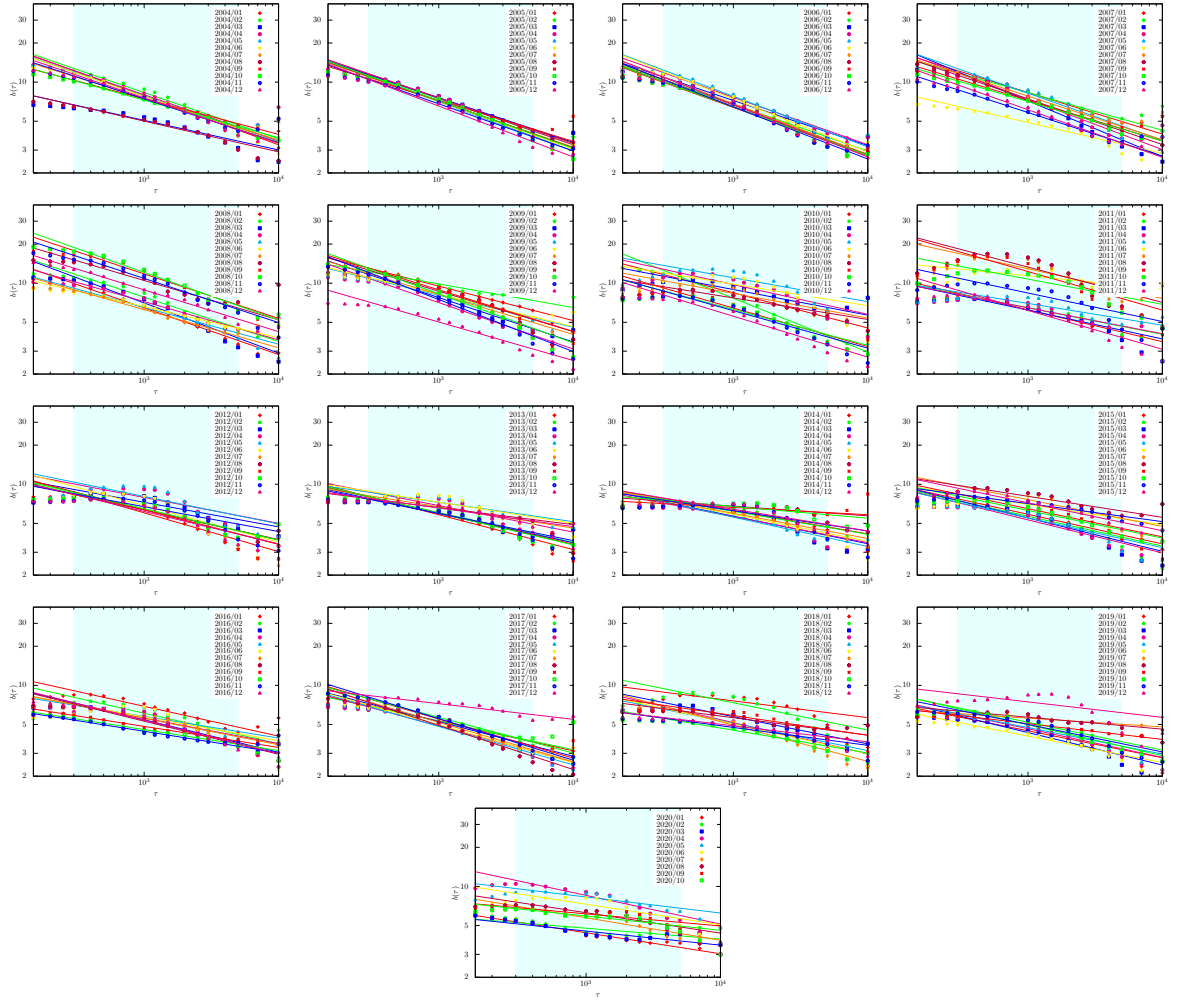


FIG. 27. Trendlines highlighting the range of τ during which the scaling phenomena is observed from 2004 to 2020. We set T_{int} 3 months and varied t_{ini} from January 2004 to December 2020 by a month.

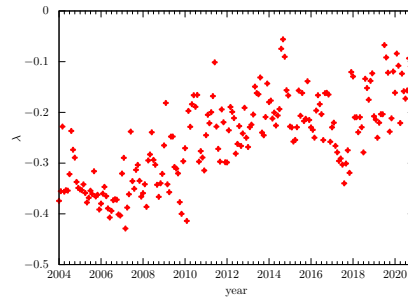


FIG. 28. Values of λ from 2004 to 2020 when the interval is 3 months.

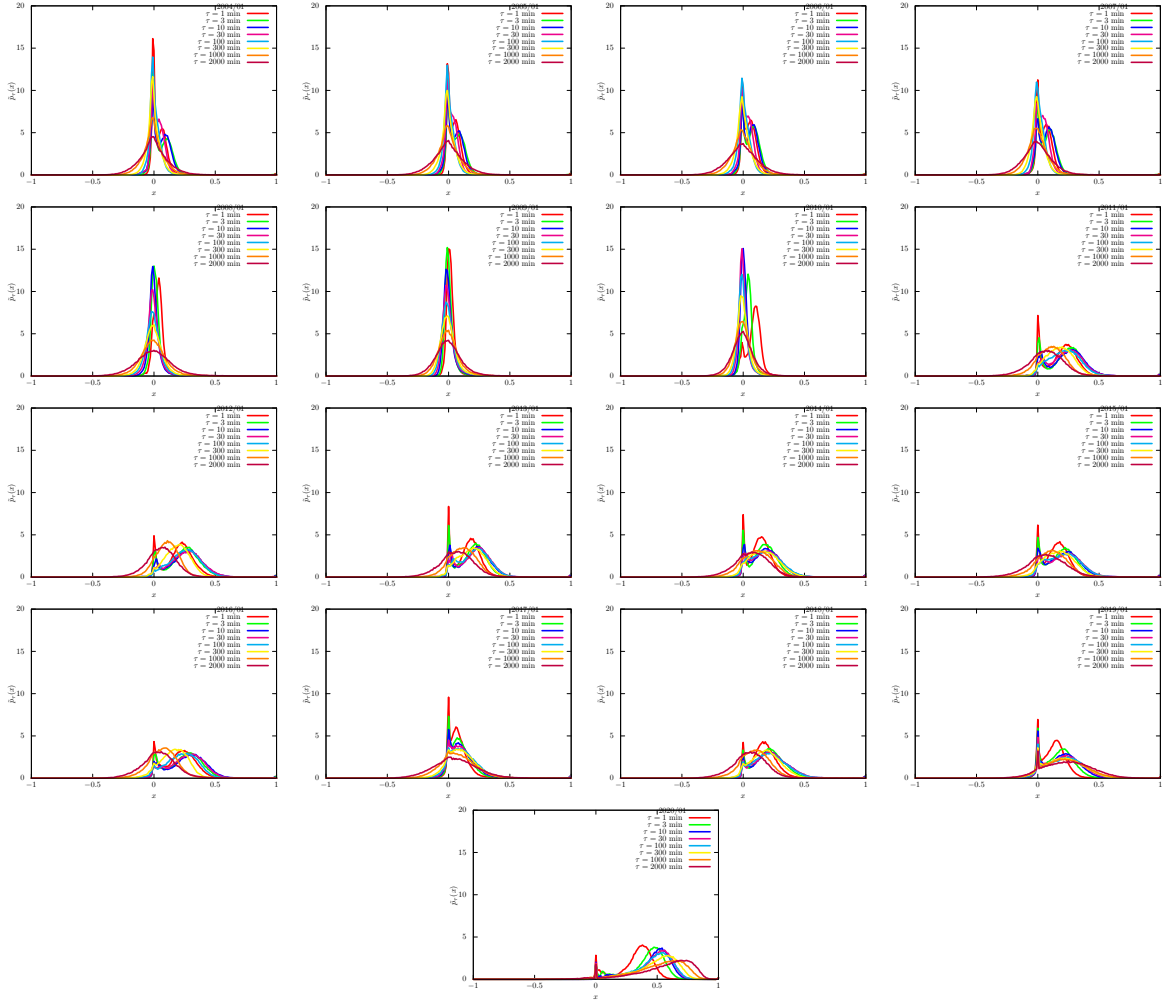


FIG. 29. Histogram $p_\tau(\cdot)$ in Eq. (II.2.1). We set T_{int} 6 months.

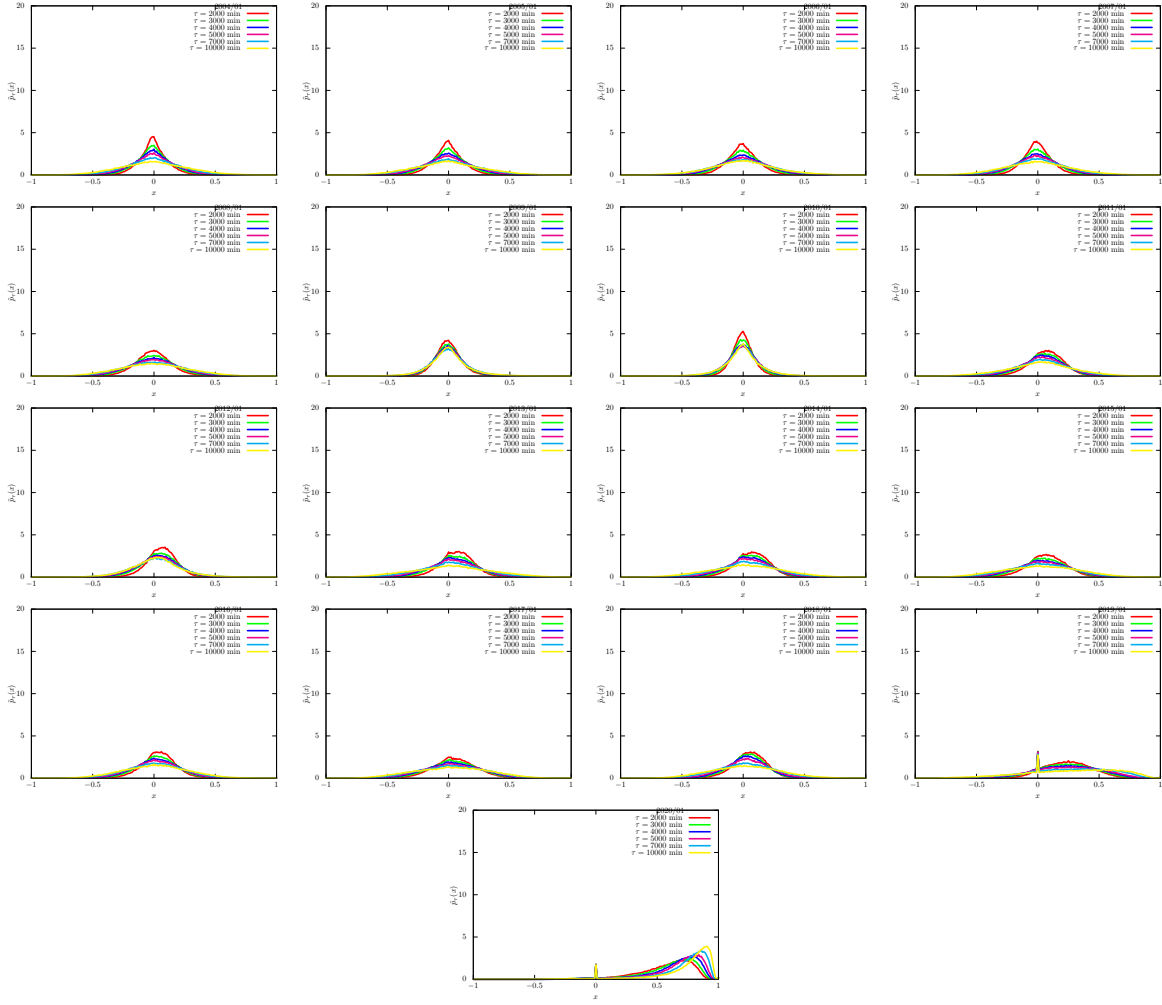


FIG. 30. Histogram $p_\tau(\cdot)$ in Eq. (II.2.1). We set T_{int} 6 months.

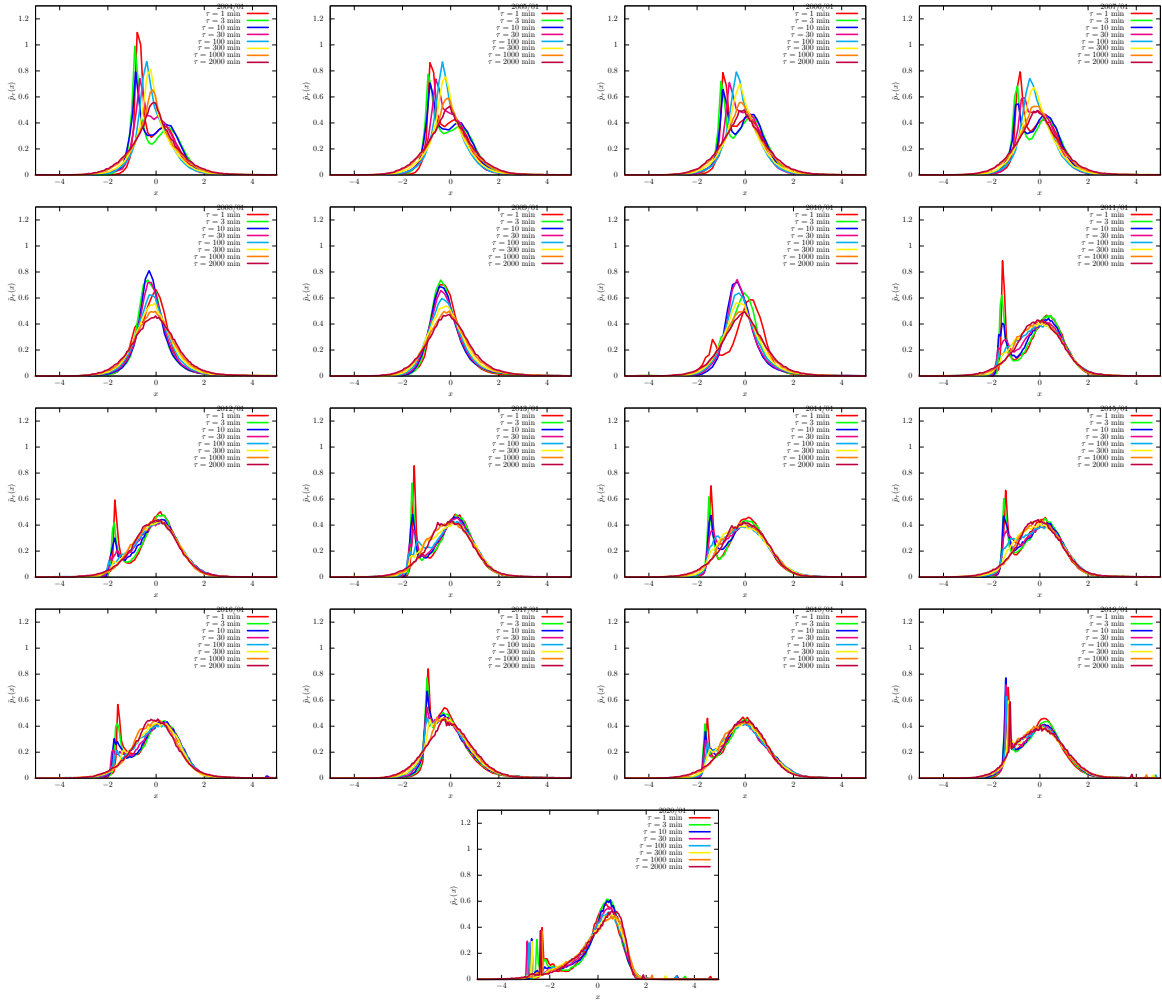


FIG. 31. Scaled histogram $\tilde{p}_\tau(\cdot)$ in Eq. (II.2.2). We set T_{int} 6 months.

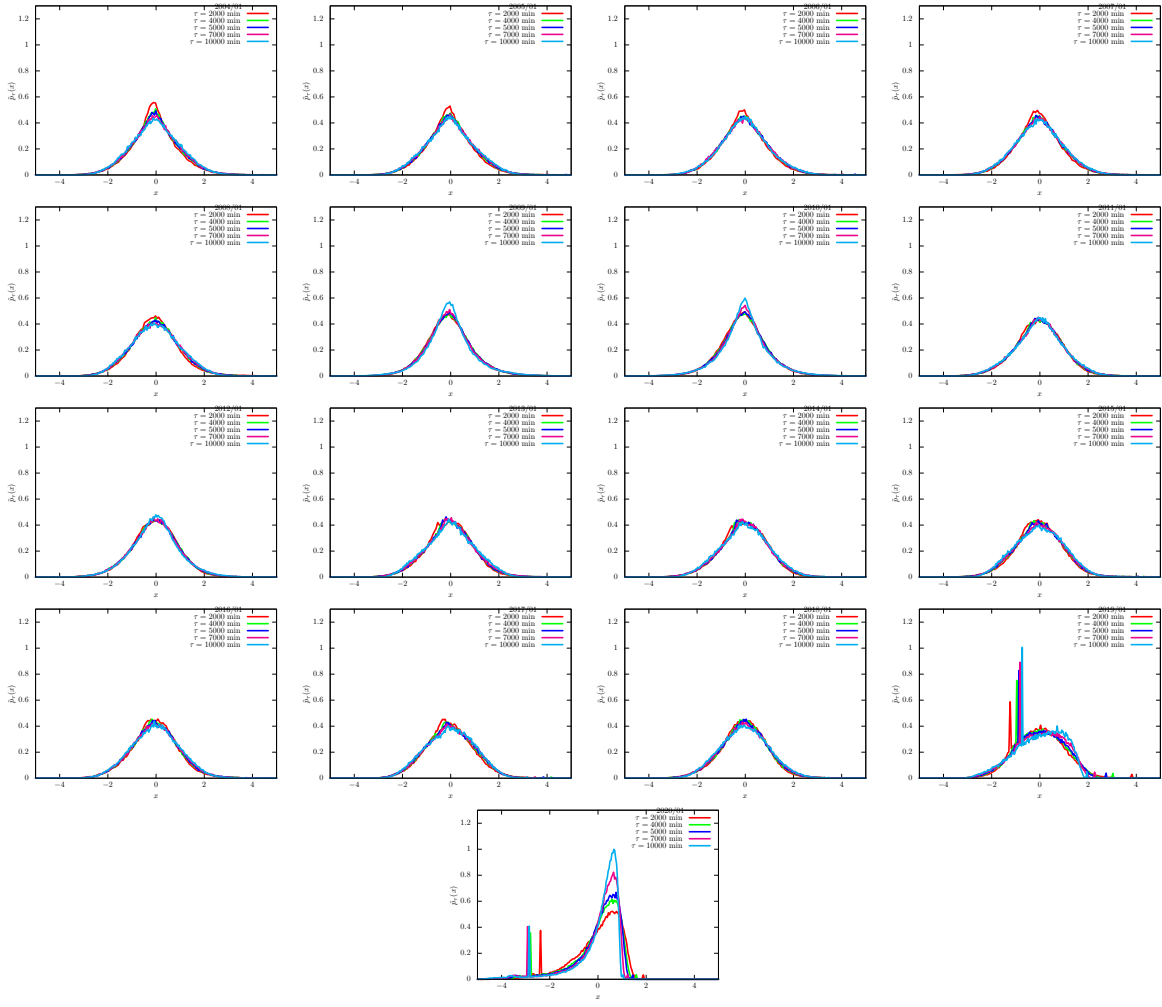


FIG. 32. Scaled histogram $\tilde{p}_\tau(\cdot)$ in Eq. (II.2.2). We set T_{int} 6 months.

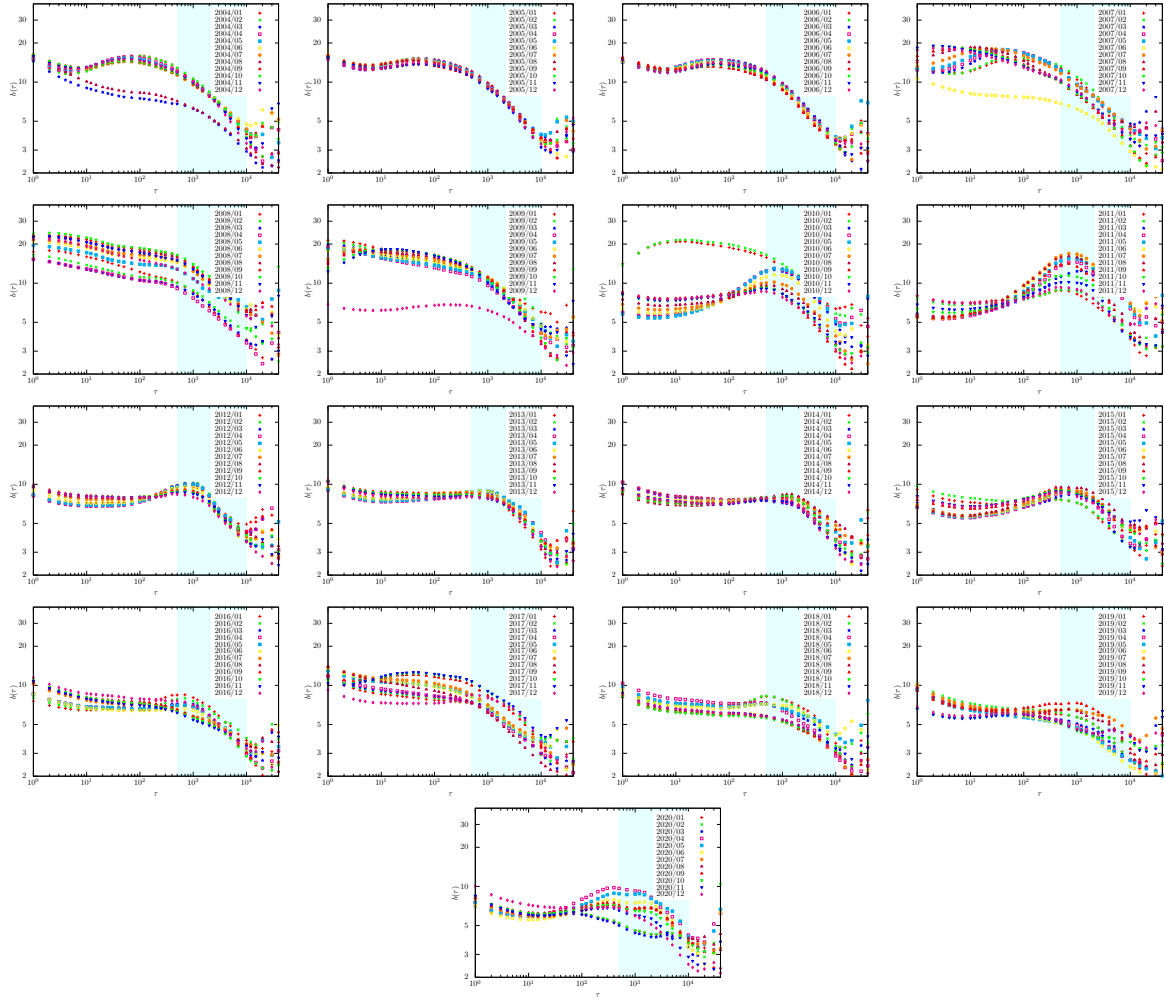


FIG. 33. Dependence of the scaling factor $b(\tau)$ on τ from 2004 to 2020. We set T_{int} 6 months and varied t_{ini} from January 2004 to December 2020 by a month.

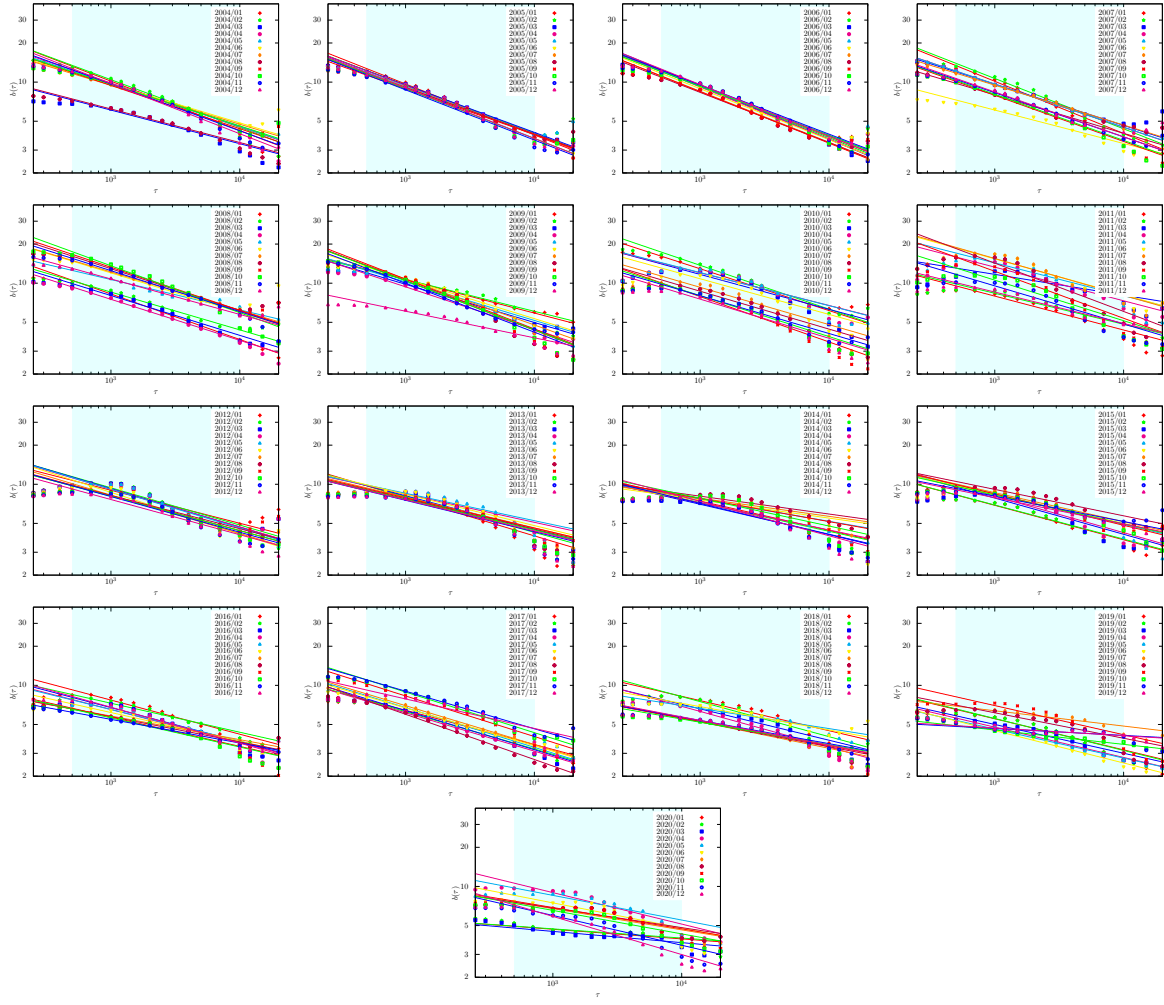


FIG. 34. Trendlines highlighting the range of τ during which the scaling phenomena is observed from 2004 to 2020. We set T_{int} 6 months and varied t_{ini} from January 2004 to December 2020 by a month.

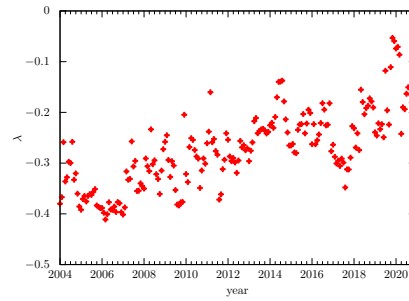


FIG. 35. Values of λ from 2004 to 2020 when the interval is 6 months.

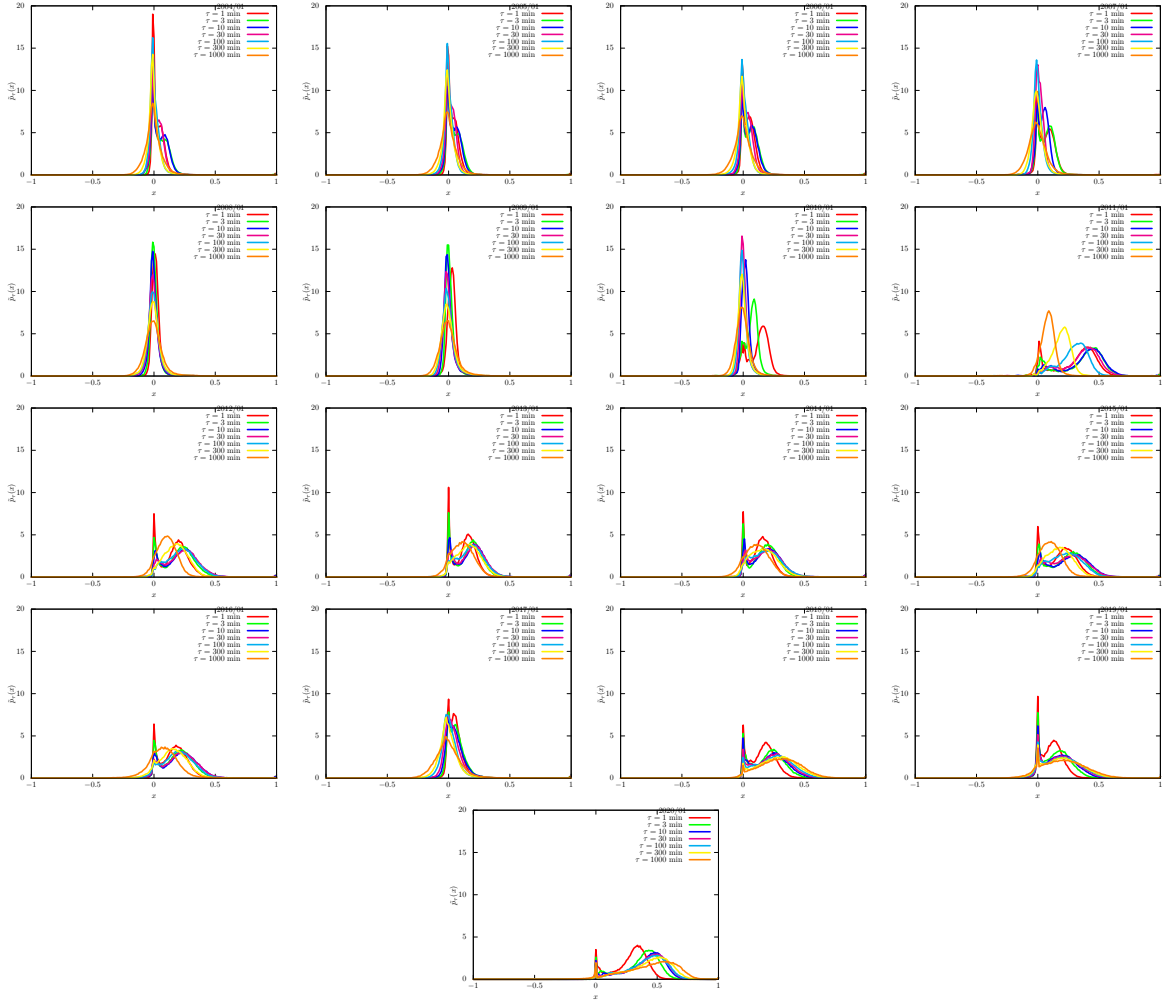


FIG. 36. Histogram $p_\tau(\cdot)$ in Eq. (II.2.1). We set T_{int} 12 months.

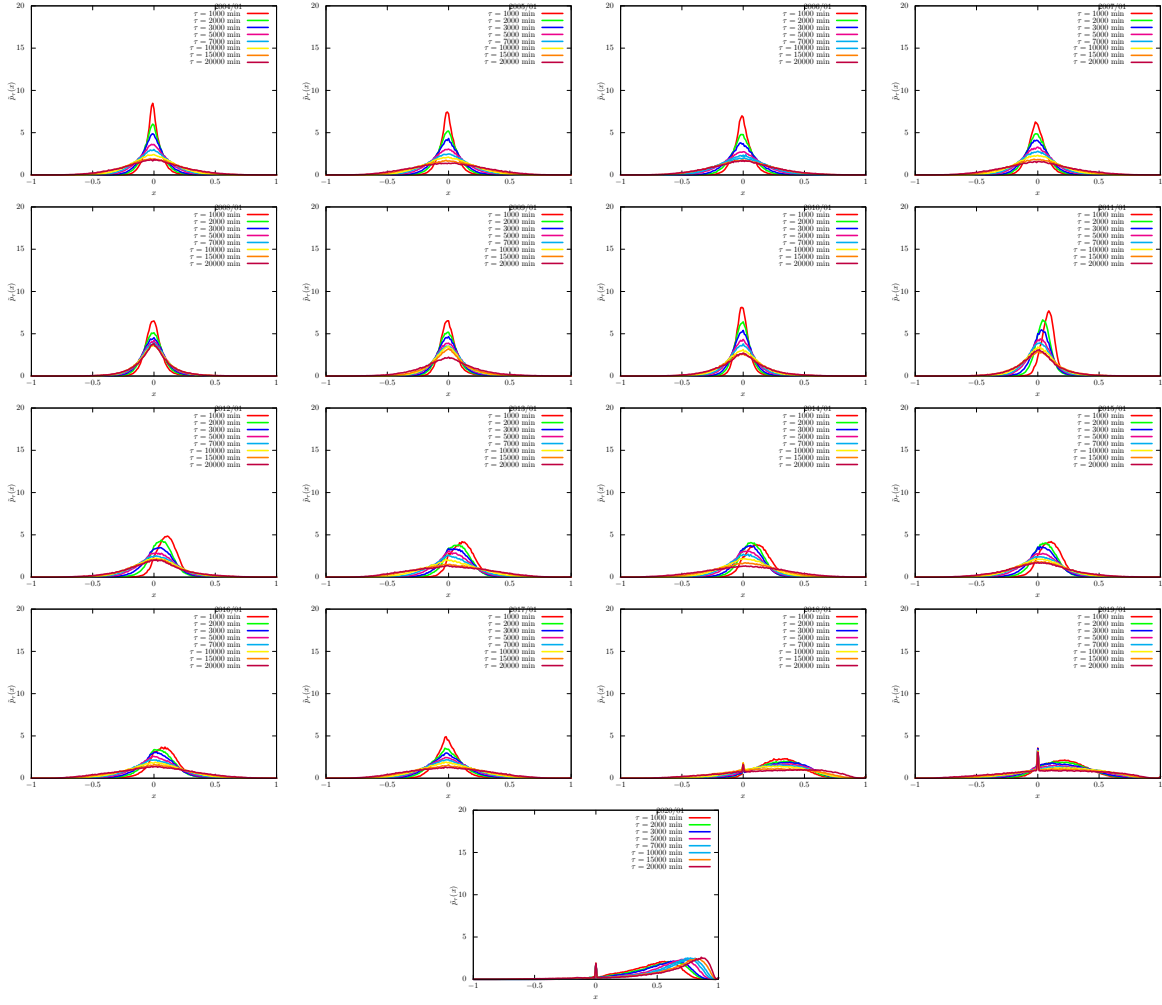


FIG. 37. Histogram $p_\tau(\cdot)$ in Eq. (II.2.1). We set T_{int} 12 months.

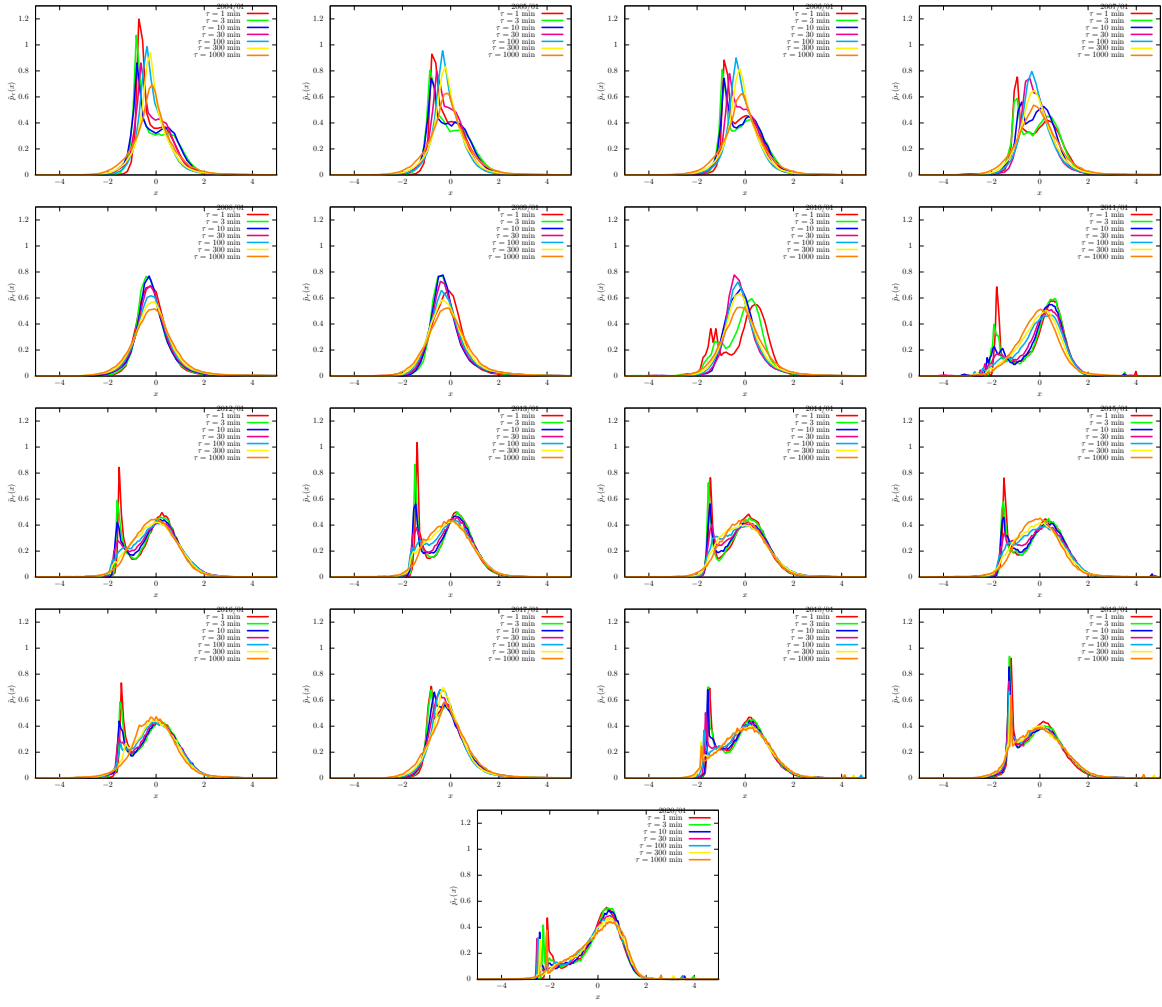


FIG. 38. Scaled histogram $\tilde{p}_\tau(\cdot)$ in Eq. (II.2.2). We set T_{int} 12 months.

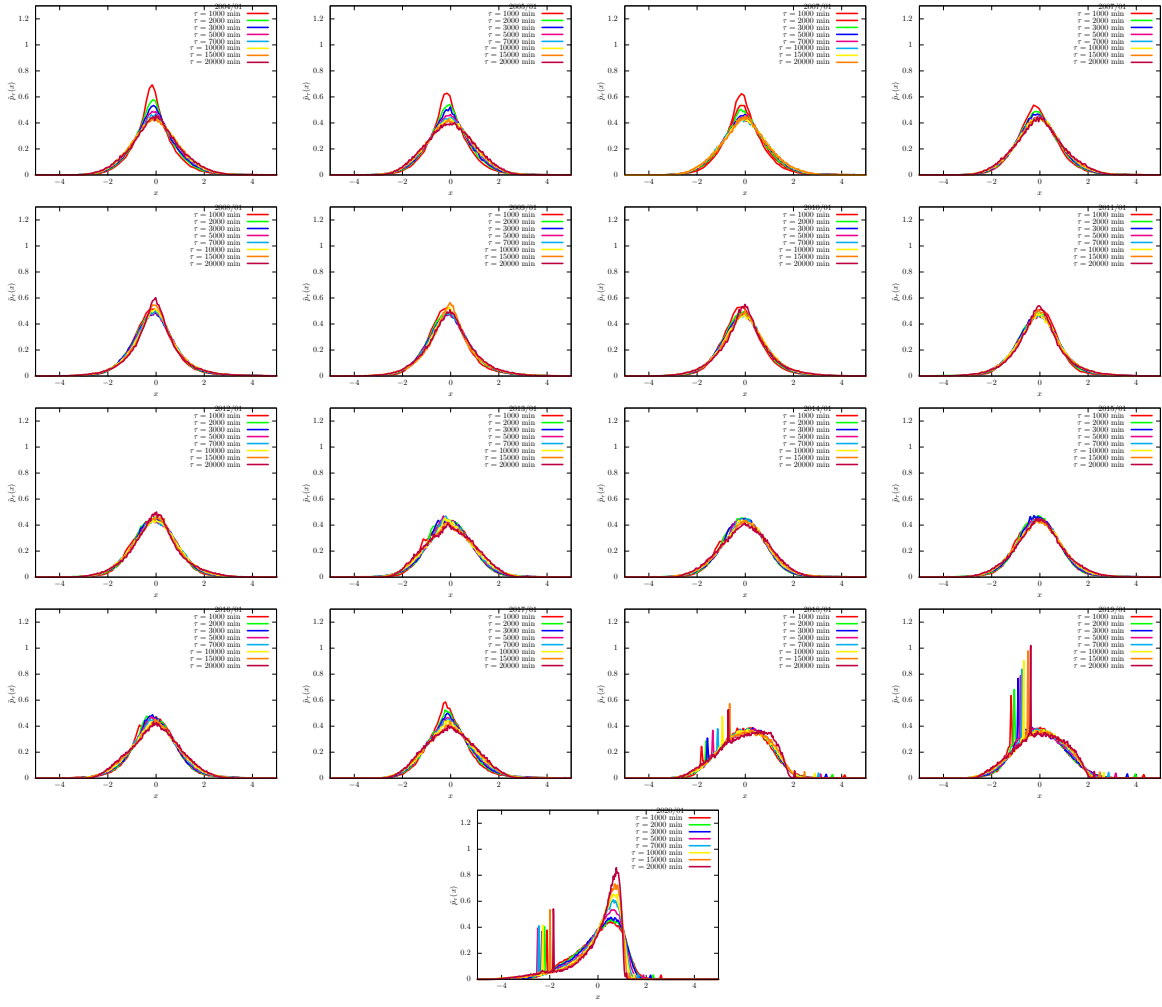


FIG. 39. Scaled histogram $\tilde{p}_\tau(\cdot)$ in Eq. (II.2.2). We set T_{int} 12 months.

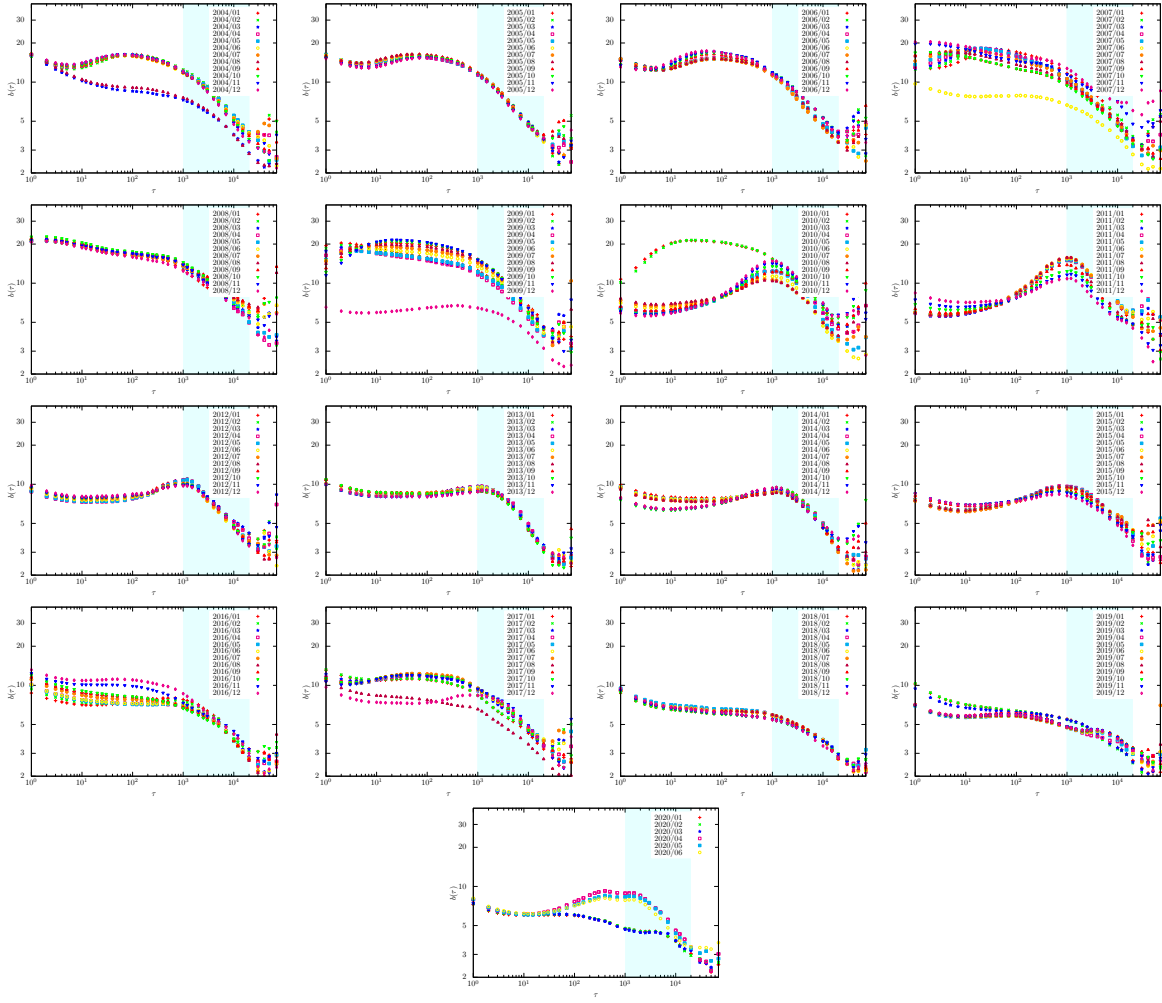


FIG. 40. Dependence of the scaling factor $b(\tau)$ on τ from 2004 to 2020. We set T_{int} 12 months and varied t_{ini} from January 2004 to December 2020 by a month.

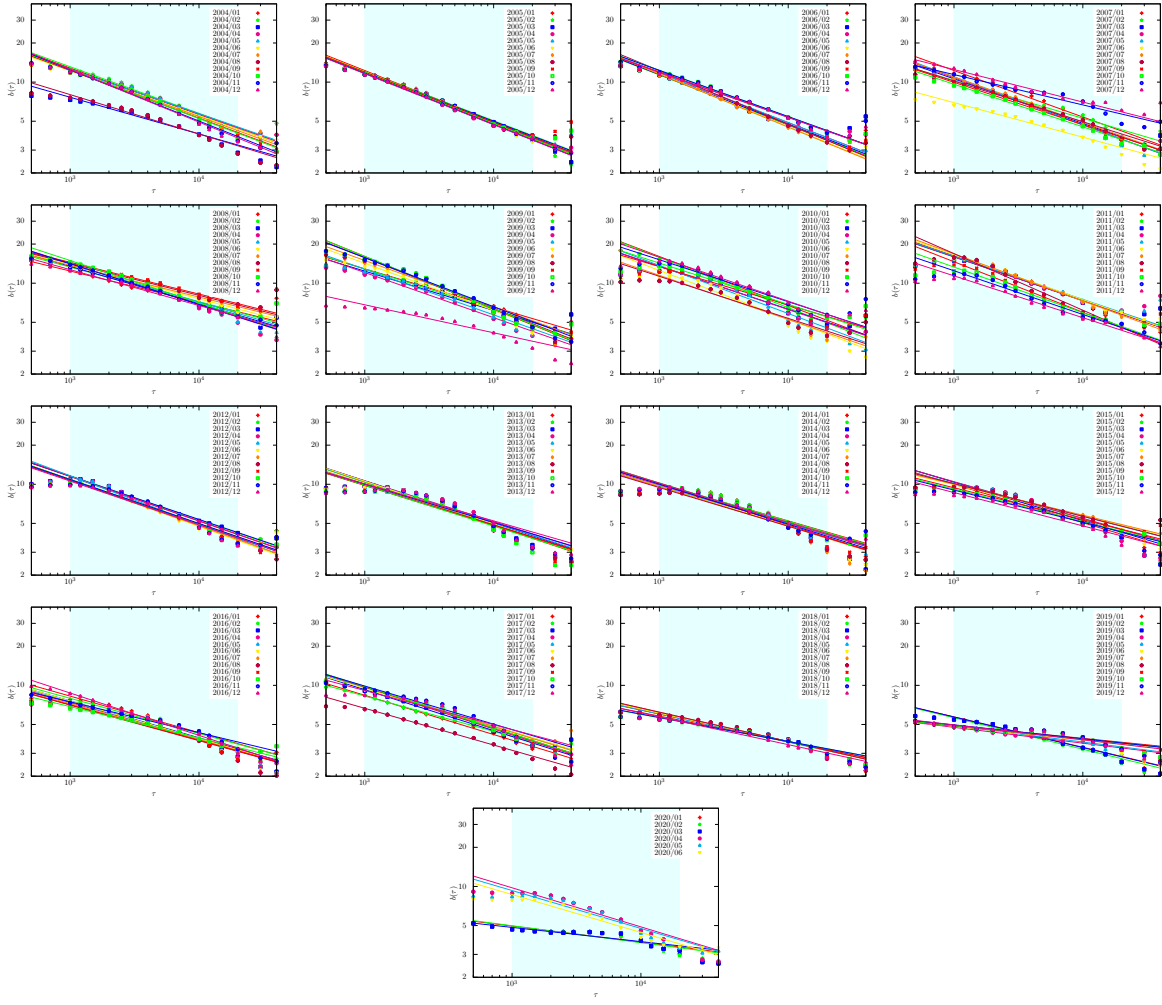


FIG. 41. Trendlines highlighting the range of τ during which the scaling phenomena is observed from 2004 to 2020. We set T_{int} 12 months and varied t_{ini} from January 2004 to December 2020 by a month.

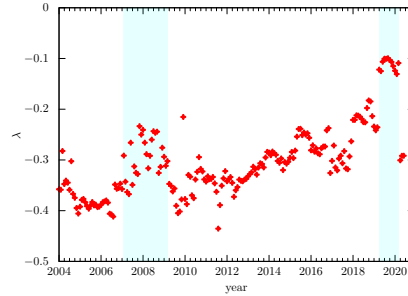


FIG. 42. Values of λ from 2004 to 2020 when the interval is 12 months. In the blue highlighted regimes, anomalies are observed. The reasons may be the market crashes called the subprime mortgage crisis and the bankruptcy of Lehman Brothers in 2007/2008 and the worldwide pandemic of COVID-19 in 2019/2020.

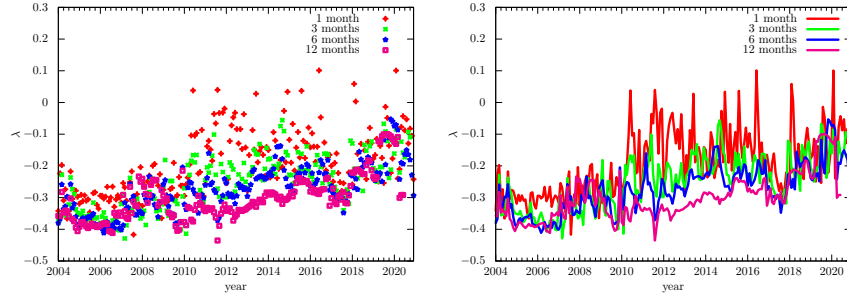


FIG. 43. Values of λ from 2004 to 2020 with the intervals of 1 month, 3 months, 6 months, and 12 months depicted via (a) points and (b) lines.

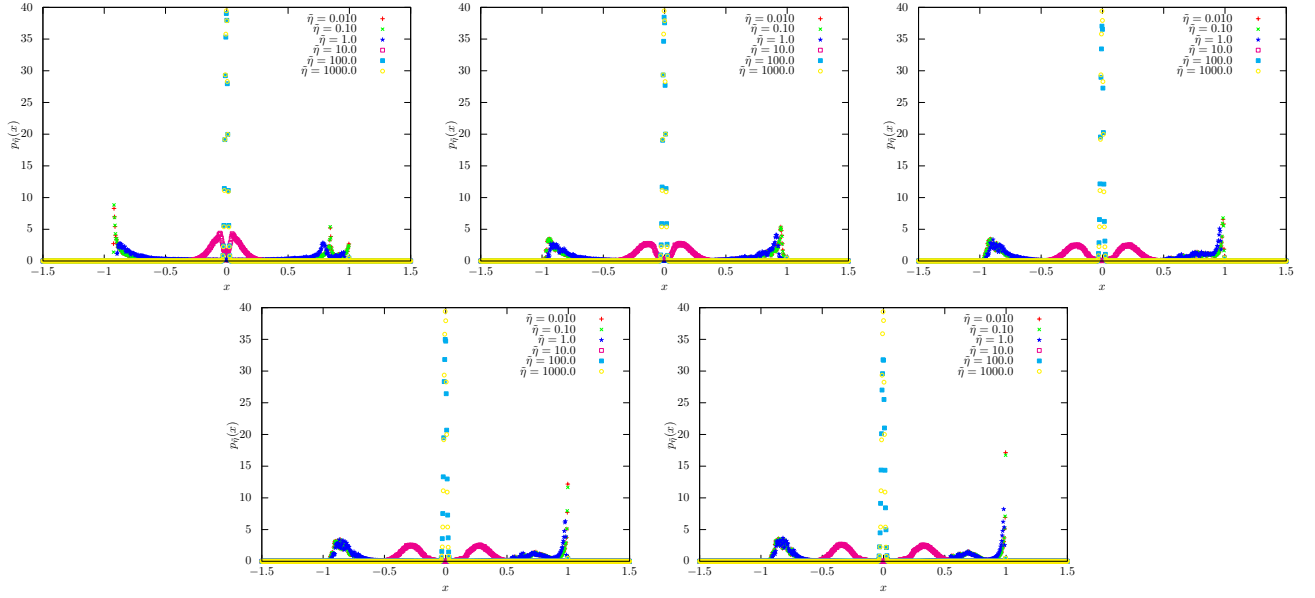


FIG. 44. Histogram $p_{\tau}(\cdot)$ in Eq. (II.2.2) of the multi-factor model. We varied $\mu_{\tilde{\gamma}}$: (a) $\mu_{\tilde{\gamma}} = 0.0$, (b) $\mu_{\tilde{\gamma}} = 0.250$, (c) $\mu_{\tilde{\gamma}} = 0.50$, (d) $\mu_{\tilde{\gamma}} = 0.75$, and (e) $\mu_{\tilde{\gamma}} = 1.0$. We set the number of steps 10000.

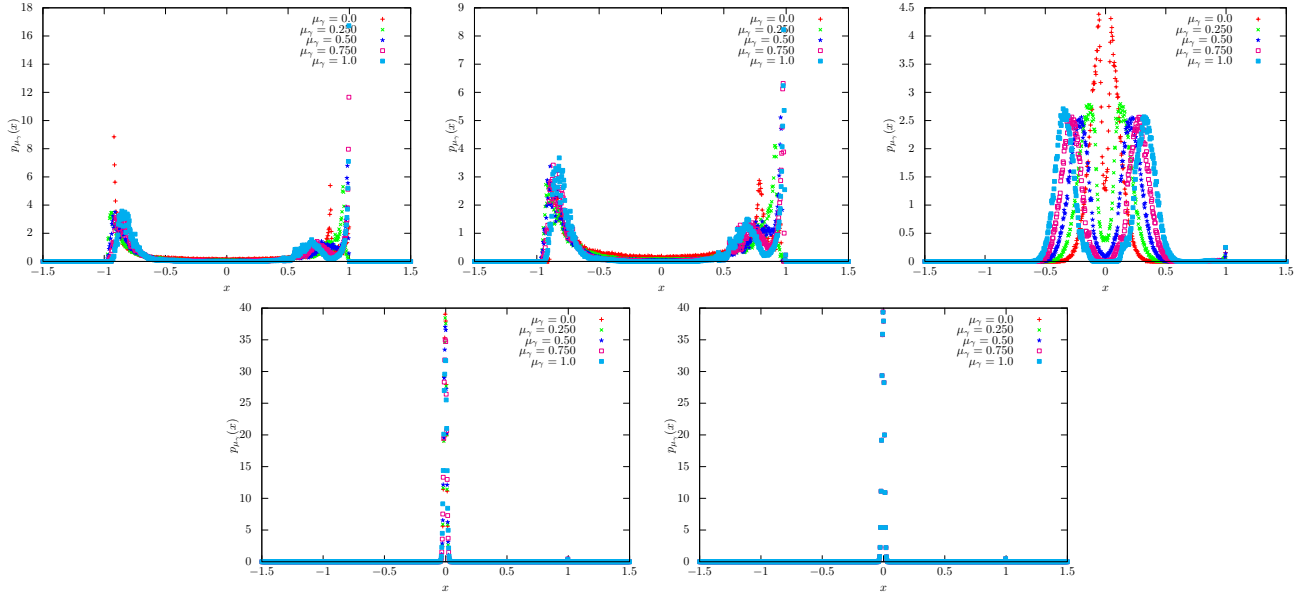


FIG. 45. Histogram $p_{\mu_{\tilde{\gamma}}}(x)$ in Eq. (II.2.2) of the multi-factor model. We varied $\tilde{\eta}$: (a) $\tilde{\eta} = 0.10$, (b) $\tilde{\eta} = 1.0$, (c) $\tilde{\eta} = 10.0$, (d) $\tilde{\eta} = 100.0$, and (e) $\tilde{\eta} = 1000.0$. We set the number of steps 10000.

Appendix B: Multi-factor model

The (scaled) histograms of the multi-factor model fail to replicate the empirical observations across the parameter space of the model (upon varying $\tilde{\eta}$, μ_{γ}). Below we present a few of these plots. In Fig. 44, we plot the histogram $p_{\tilde{\eta}}(x)$ in Eq. (II.2.1) of the multi-factor model across multiple values of $\tilde{\eta}$ for fixed values of μ_{γ} . Note that the subscript is changed from τ to $\tilde{\eta}$. In Fig. 45, we plot the equivalent histograms $p_{\tilde{\eta}}(x)$ across multiple values of μ_{γ} for fixed values of $\tilde{\eta}$. The respective scaled versions are presented in Figs. 46, 47. In Fig. 47, we plot the scaled histogram $\tilde{p}_{\tilde{\eta}}(x)$ in Eq. (II.2.2) of the multi-factor model.

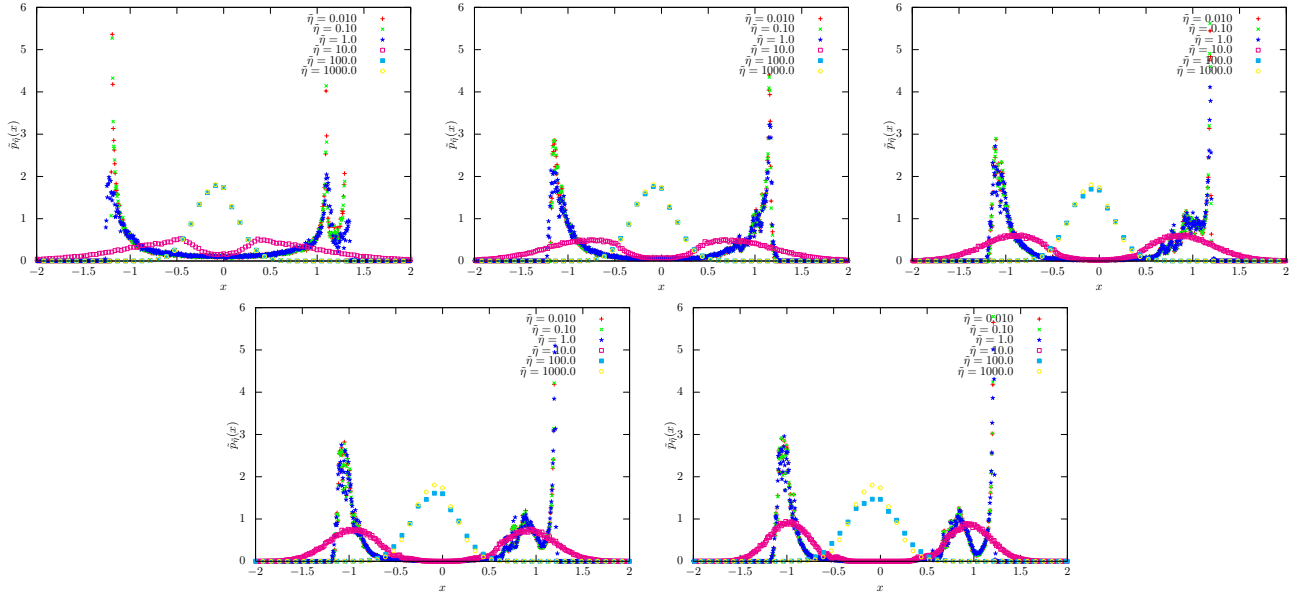


FIG. 46. Scaled histogram $\tilde{p}_{\tilde{\eta}}(\cdot)$ in Eq. (II.2.2) of the multi-factor model. We varied $\mu_{\tilde{\gamma}}$: (a) $\mu_{\tilde{\gamma}} = 0.0$, (b) $\mu_{\tilde{\gamma}} = 0.250$, (c), $\mu_{\tilde{\gamma}} = 0.50$, (d) $\mu_{\tilde{\gamma}} = 0.75$, and (e) $\mu_{\tilde{\gamma}} = 1.0$. We set the number of steps 10000.

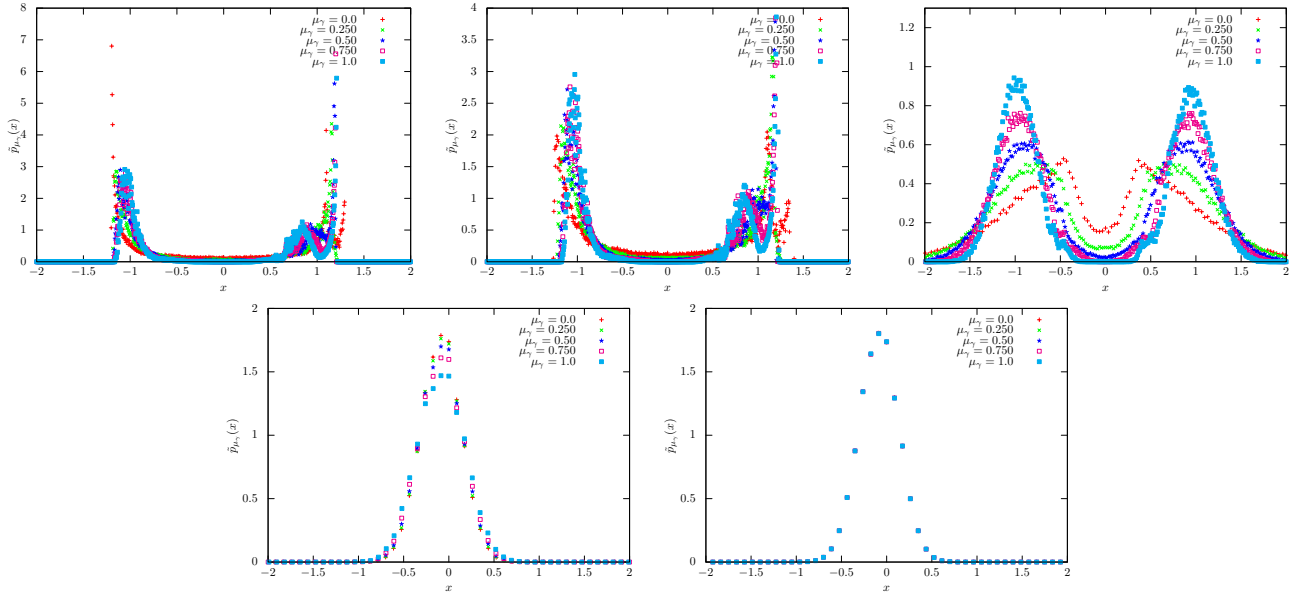


FIG. 47. Scaled histogram $\tilde{p}_{\mu_{\tilde{\gamma}}}(x)$ in Eq. (II.2.2) of the multi-factor model. We varied $\tilde{\eta}$: (a) $\tilde{\eta} = 0.10$, (b) $\tilde{\eta} = 1.0$, (c) $\tilde{\eta} = 10.0$, (d) $\tilde{\eta} = 100.0$, and (e) $\tilde{\eta} = 1000.0$. We set the number of steps 10000.

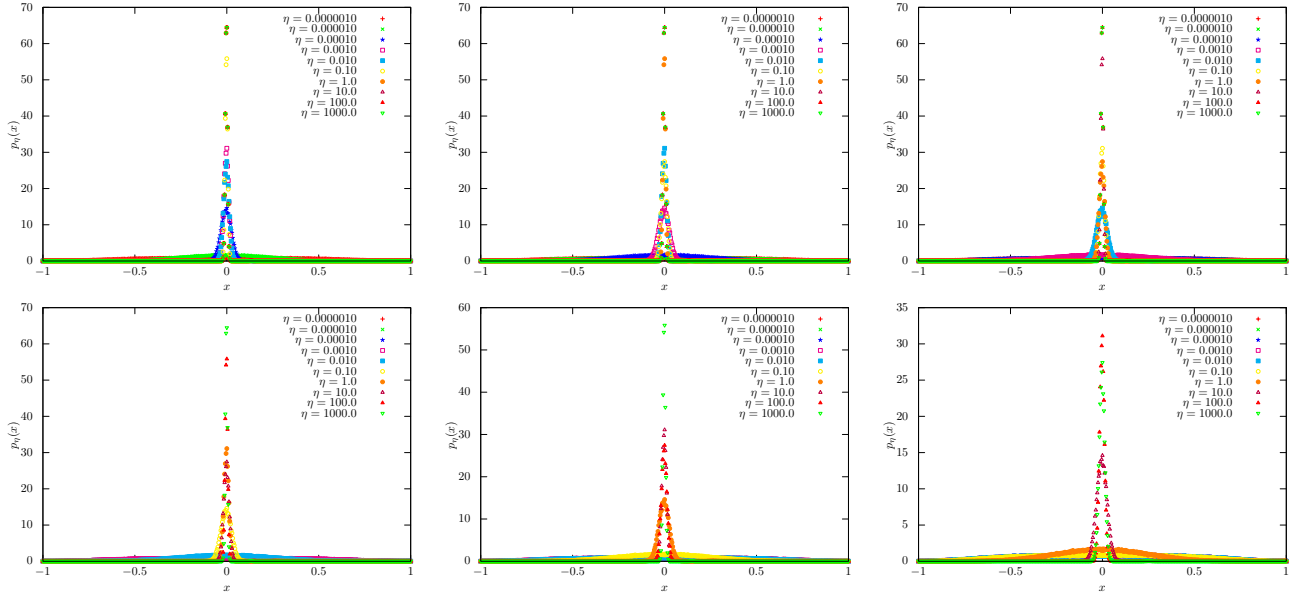


FIG. 48. Histogram $p_\eta(x)$ in Eq. (II.2.2) of the modified Vicsek model. Note that the subscript is changed from τ to η . We varied δ : (a) $\delta = 0.010$, (b) $\delta = 0.10$, (c) $\delta = 1.0$, (d) $\delta = 10.0$, (e) $\delta = 100.0$, and (f) 1000.0 . We set the number of steps 10000.

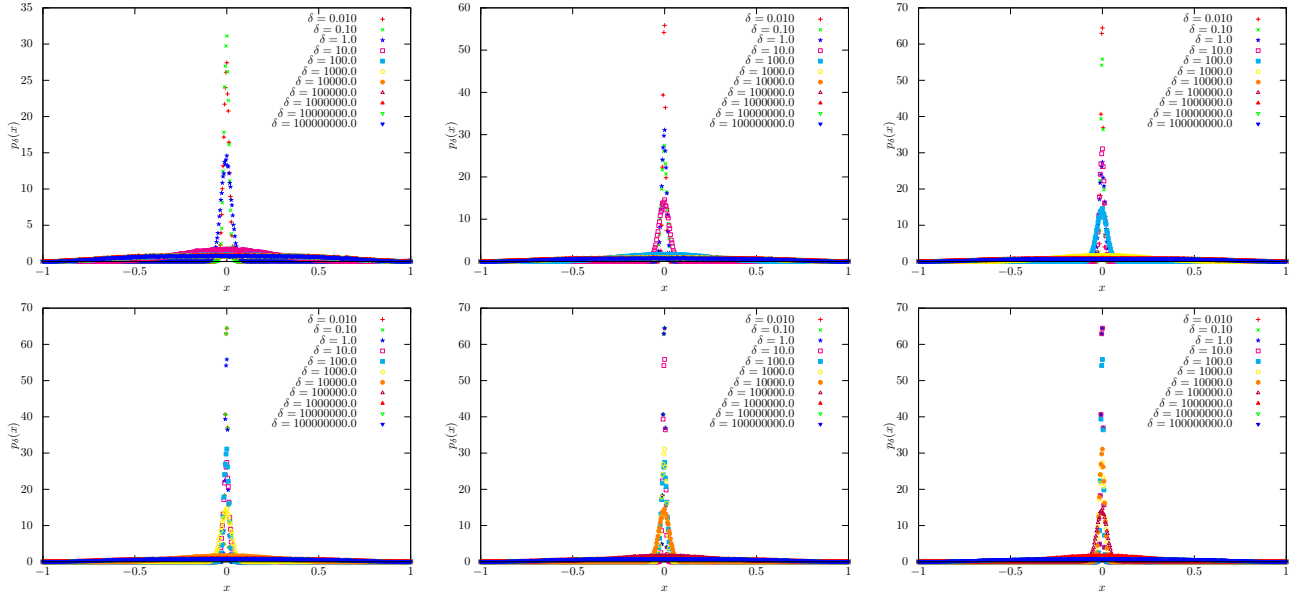


FIG. 49. Histogram $p_\delta(x)$ in Eq. (II.2.2) of the modified Vicsek model. Note that the subscript is changed from τ to δ . We varied η : (a) $\eta = 0.010$, (b) $\eta = 0.10$, (c) $\eta = 1.0$, (d) $\eta = 10.0$, (e) $\eta = 100.0$, and (f) $\eta = 1000.0$. We set the number of steps 10000.

Appendix C: Modified Vicsek model

Similar to the experiments conducted on the multi-factor model, in this case, we identify the key parameters as η and δ . We shows that across several combinations of parameters, the modified Vicsek model demonstrates the two emergent phenomena: a. Scaling of $b(\tau)$ w.r.t τ ; and b. A stable functional form during the scaling regime.

In Figs. 48, 49 we plot the histograms $p_\eta(x)$ for different fixed values of δ and $p_\delta(x)$ for different fixed values of η . Figs. 50, 51 show the respective scaled forms.

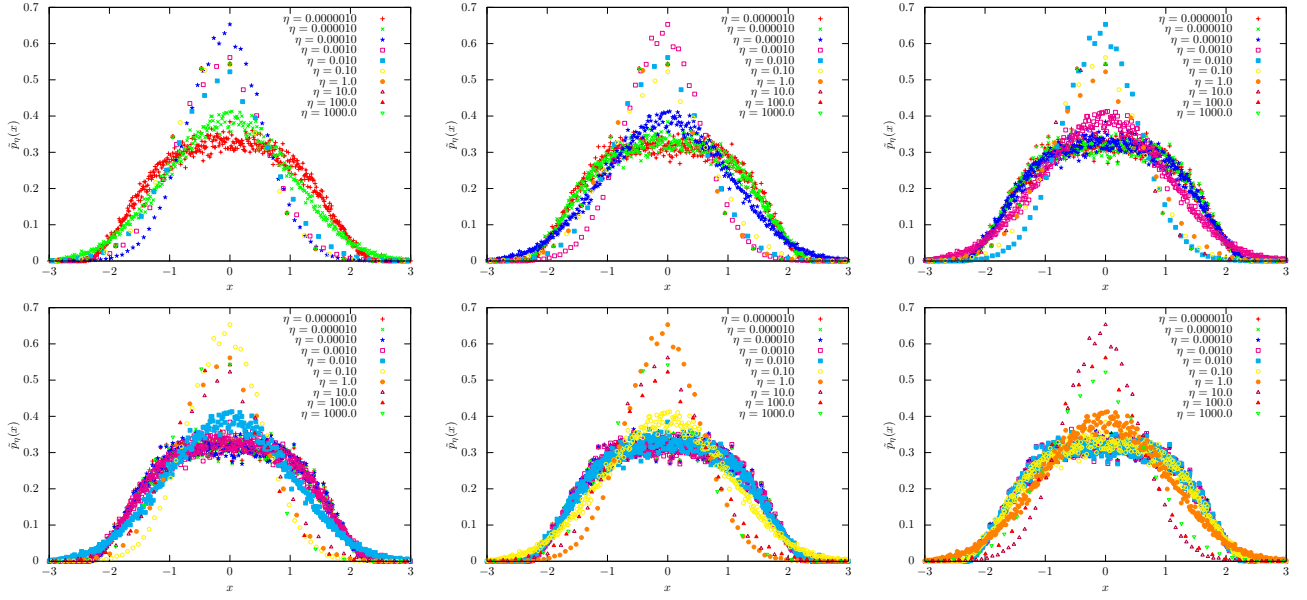


FIG. 50. Scaled histogram $\tilde{p}_\eta(x)$ in Eq. (II.2.2) of the modified Vicsek model. Note that the subscript is changed from τ to η . We varied δ : (a) $\delta = 0.010$, (b) $\delta = 0.10$, (c) $\delta = 1.0$, (d) $\delta = 10.0$, (e) $\delta = 100.0$, and (f) 1000.0 . We set the number of steps 10000.

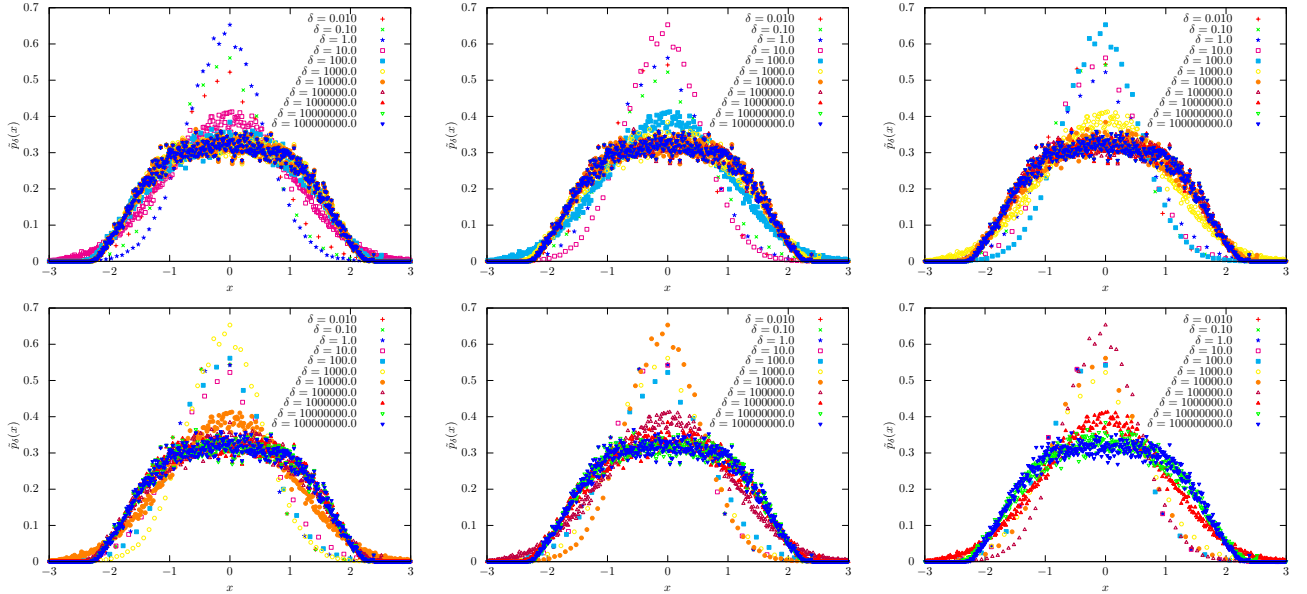


FIG. 51. Scaled histogram $\tilde{p}_\delta(x)$ in Eq. (II.2.2) of the modified Vicsek model. Note that the subscript is changed from τ to δ . We varied η : (a) $\eta = 0.010$, (b) $\eta = 0.10$, (c) $\eta = 1.0$, (d) $\eta = 10.0$, (e) $\eta = 100.0$, and (f) $\eta = 1000.0$. We set the number of steps 10000.

1. Relationship between parameters of the modified Vicsek model and the standard deviation of histograms

In Fig. 52, we plot the relationship between η and the scaling factor $b(\cdot)$ and that between δ and the scaling factor.

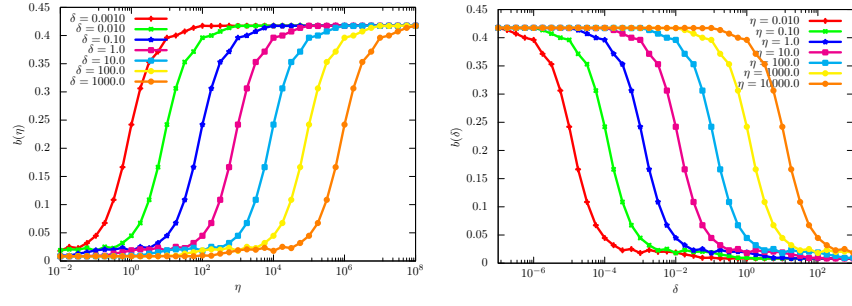


FIG. 52. (a) The relationship between η in the modified Vicsek model and $b(\eta)$, which is the scale factor. Note that we changed the argument from τ to η . We set the number of steps 10000. (b) The relationship between δ in the modified Vicsek model and $b(\delta)$, which is the scale factor. Note that we changed the argument from τ to δ . We set the number of steps 10000.

Appendix D: Derivation of the modified Vicsek model

In the main text, we investigated the modified Vicsek model though we did not show its derivation. In this section, we show the derivation of the modified Vicsek model.

1. Vicsek model and its variants

We first explain the Vicsek model [26]. The Vicsek model was proposed as a possible candidate to explain bird flocking and succeeded in describing the phase transition that particles form a flock. Then, we rewrite it in the form of a continuous-time system.

a. Vicsek model

Here we give the definition of the Vicsek model. Let us consider a two-dimensional system of N kinetic particles. We denote, by $\vec{x}_i(t)$ and $\vec{v}_i(t)$, the position and velocity of particle i at time t . The position of i is updated by

$$\vec{x}_i(t + \Delta t) = \vec{x}_i(t) + \vec{v}_i(t)\Delta t. \quad (\text{D.1.1})$$

The amplitude of the velocity of each particle is constant: $\|\vec{v}_i(t)\|_{\text{F}} = v_{\text{abs}}$. But the direction of $\vec{v}_i(t)$ is update by

$$\vec{v}_i(t) = v_{\text{abs}} \begin{bmatrix} \cos \theta_i(t) \\ \sin \theta_i(t) \end{bmatrix}, \quad (\text{D.1.2})$$

and

$$\theta_i(t + \Delta t) = \frac{1}{N_{i,\delta}} \sum_{j: \|\vec{x}_i(t) - \vec{x}_j(t)\|_{\text{F}} < \delta} \theta_j(t) + \Xi_i(t), \quad (\text{D.1.3})$$

$$\Xi_i(t) \sim [-\eta/2, \eta/2], \quad (\text{D.1.4})$$

where $N_{i,\delta}$ is the number of elements j that satisfy $\|\vec{x}_i(t) - \vec{x}_j(t)\|_{\text{F}} < \delta$. Instead of the uniform distribution, we can use the normal distribution for $\Xi_i(t)$:

$$\Xi_i(t) \sim \mathcal{N}\left(0, \frac{\eta^2}{12}\right). \quad (\text{D.1.5})$$

b. Continuous version of the Vicsek model

The continuous variant of Eqs. (D.1.1), (D.1.2), and (D.1.4), takes the form

$$\frac{d}{dt} \vec{x}_i(t) = \vec{v}_i(t), \quad (\text{D.1.6})$$

where

$$\vec{v}_i(t) = v_{\text{abs}} \begin{bmatrix} \cos \theta_i(t) \\ \sin \theta_i(t) \end{bmatrix}, \quad (\text{D.1.7})$$

$$\dot{\theta}_i(t) = -\alpha_i \theta_i(t) + \frac{\beta_i}{N_{i,\delta}} \sum_{j: \|\vec{x}_i(t) - \vec{x}_j(t)\|_{\text{F}} < \delta} \theta_j(t) + \xi_i(t). \quad (\text{D.1.8})$$

Taking the time-derivative of Eq. (D.1.6), we can transform it into

$$\dot{\vec{v}}_i(t) = v_{\text{abs}} \begin{bmatrix} -\sin \theta_i(t) \\ \cos \theta_i(t) \end{bmatrix} \dot{\theta}_i(t) \quad (\text{D.1.9})$$

$$= v_{\text{abs}} \begin{bmatrix} -\sin \theta_i(t) \\ \cos \theta_i(t) \end{bmatrix} \left(-\alpha_i \theta_i(t) + \frac{\beta_i}{N_{i,\delta}} \sum_{j: \|\vec{x}_i(t) - \vec{x}_j(t)\|_{\text{F}} < \delta} \theta_j(t) + \xi_i(t) \right). \quad (\text{D.1.10})$$

Again, we discretize the above equations, Eqs. (D.1.6), (D.1.7), and (D.1.7):

$$\vec{x}_i(t + \Delta t) = \vec{x}_i(t) + \vec{v}_i(t)\Delta t, \quad (\text{D.1.11})$$

where

$$\vec{v}_i(t) = v_{\text{abs}} \begin{bmatrix} \cos \theta_i(t) \\ \sin \theta_i(t) \end{bmatrix}, \quad (\text{D.1.12})$$

and

$$\theta_i(t + \Delta t) = \theta_i(t) + \left(-\alpha_i \theta_i(t) + \frac{\beta_i}{N_{i,\delta}} \sum_{j: \|\vec{x}_i(t) - \vec{x}_j(t)\|_{\text{F}} < \delta} \theta_j(t) + \xi_i(t) \right) \Delta t \quad (\text{D.1.13})$$

$$= (1 - \alpha_i \Delta t) \theta_i(t) + \frac{\beta_i \Delta t}{N_{i,\delta}} \sum_{j: \|\vec{x}_i(t) - \vec{x}_j(t)\|_{\text{F}} < \delta} \theta_j(t) + \xi_i(t) \Delta t. \quad (\text{D.1.14})$$

To recover the original equation of $\theta_i(t)$, Eq. (D.1.4), we need to set $\alpha_i = \frac{1}{\Delta t}$ and $\beta_i = \frac{1}{\Delta t}$. To summarize the above equations, Eqs. (D.1.11), (D.1.12), and (D.1.14), we get

$$\vec{v}_i(t + \Delta t) = \vec{v}_i(t) + v_{\text{abs}} \begin{bmatrix} -\sin \theta_i(t) \\ \cos \theta_i(t) \end{bmatrix} \left(-\alpha_i \theta_i(t) + \frac{\beta_i}{N_{i,\delta}} \sum_{j: \|\vec{x}_i(t) - \vec{x}_j(t)\|_{\text{F}} < \delta} \theta_j(t) + \xi_i(t) \right) \Delta t \quad (\text{D.1.15})$$

$$= v_{\text{abs}} \begin{bmatrix} \cos \theta_i(t) \\ \sin \theta_i(t) \end{bmatrix} + v_{\text{abs}} \begin{bmatrix} -\sin \theta_i(t) \\ \cos \theta_i(t) \end{bmatrix} \left(-\alpha_i \theta_i(t) + \frac{\beta_i}{N_{i,\delta}} \sum_{j: \|\vec{x}_i(t) - \vec{x}_j(t)\|_{\text{F}} < \delta} \theta_j(t) + \xi_i(t) \right) \Delta t. \quad (\text{D.1.16})$$

2. The Modified Vicsek model

By introducing the interaction terms in Eq. (D.1.10) into free particles described by the Langevin equation, we propose the following model:

$$\dot{r}_i(t) = v_i(t), \quad (\text{D.2.1a})$$

$$m_i \dot{v}_i(t) = -\alpha_i v_i(t) - \beta_i r_i(t) + \frac{\gamma_i}{N_{i,\delta}} \sum_{j: |r_i(t) - r_j(t)| < \delta} v_j(t) + \xi_i(t), \quad (\text{D.2.1b})$$

where $N_{i,\delta}$ is the number of elements j that satisfy $|r_i(t) - r_j(t)| < \delta$ and

$$\xi_i(t) := \frac{d}{dt} \Xi_i(t, \cdot). \quad (\text{D.2.2})$$

Here we call Eq. (D.2.1) the modified Vicsek model. Note that $v_i(t)$ is included in $\sum_{j: |r_i(t) - r_j(t)| < \delta} v_j(t)$ if $\delta > 0$ and the summation is zero if $\delta = 0$. Here, for $t \geq t'$, $\Xi(t, t')$ obeys

$$\Xi_i(t, t') \sim \mathcal{N}(0, \eta_i^2(t - t')). \quad (\text{D.2.3})$$

Note that, in the case of the Langevin equation, we have $\eta_i^2 = 2\gamma k_{\text{B}} T$.

For numerical simulations, we simplify Eq. (D.2.1). Unifying the two equations, Eq. (D.2.1), we obtain

$$m_i \ddot{r}_i(t) = -\alpha_i \dot{r}_i(t) - \beta_i r_i(t) + \frac{\gamma_i}{N_{i,\delta}} \sum_{j: |r_i(t) - r_j(t)| < \delta} \dot{r}_j(t) + \xi_i(t). \quad (\text{D.2.4})$$

Taking the overdamped limit $m_i \rightarrow 0$, we get

$$\alpha_i \dot{r}_i(t) = -\beta_i r_i(t) + \frac{\gamma_i}{N_{i,\delta}} \sum_{j: |r_i(t) - r_j(t)| < \delta} \dot{r}_j(t) + \xi_i(t). \quad (\text{D.2.5})$$

By discretizing Eq. (D.2.5), we have

$$\alpha_i r_i(t + \Delta t) = (\alpha_i - \beta_i \Delta t) r_i(t) + \frac{\gamma_i}{N_{i,\delta}} \sum_{j: |r_i(t) - r_j(t)| < \delta} (r_j(t + \Delta t) - r_j(t)) + \Xi_i(t + \Delta t, t). \quad (\text{D.2.6})$$

However, it is time-consuming to solve Eq. (D.2.6) since it involves a backward term. Assuming $r_j(t + \Delta t) - r_j(t) = r_j(t) - r_j(t - \Delta t)$, we have

$$\alpha_i r_i(t + \Delta t) = (\alpha_i - \beta_i \Delta t) r_i(t) + \frac{\gamma_i}{N_{i,\delta}} \sum_{j: |r_i(t) - r_j(t)| < \delta} (r_j(t) - r_j(t - \Delta t)) + \Xi_i(t + \Delta t, t). \quad (\text{D.2.7})$$

Finally, we obtained Eq. (IV.2.1).

-
- [1] M. E. J. Newman, Resource letter cs-1: Complex systems, American Journal of Physics **79**, 800 (2011), <https://doi.org/10.1119/1.3590372>.
 - [2] J. Ladyman, J. Lambert, and K. Wiesner, What is a complex system?, European Journal for Philosophy of Science **3**, 33 (2013).
 - [3] J. Ladyman and K. Wiesner, *What is a complex system?* (Yale University Press, 2020).
 - [4] R. N. Mantegna and H. E. Stanley, *Introduction to econophysics: correlations and complexity in finance* (Cambridge university press, 1999).
 - [5] G. Bonanno, F. Lillo, and R. N. Mantegna, Levels of complexity in financial markets, Physica A: Statistical Mechanics and its Applications **299**, 16 (2001).
 - [6] J.-P. Bouchaud, The subtle nature of financial random walks, Chaos: An Interdisciplinary Journal of Nonlinear Science **15**, 026104 (2005).
 - [7] H. Stanley, X. Gabaix, P. Gopikrishnan, and V. Plerou, Economic fluctuations and statistical physics: Quantifying extremely rare and less rare events in finance, Physica A: Statistical Mechanics and its Applications **382**, 286 (2007).
 - [8] M. S. Rozeff and W. R. Kinney, Capital market seasonality: The case of stock returns, Journal of Financial Economics **3**, 379 (1976).
 - [9] B. Mandelbrot, P. Cootner, R. Gomory, E. Fama, W. Morris, and H. Taylor, *Fractals and Scaling in Finance: Discontinuity, Concentration, Risk. Selecta Volume E*, SpringerLink : Bücher (Springer New York, 2013).
 - [10] F. Luna and A. Perrone, *Agent-based methods in economics and finance: simulations in Swarm*, Vol. 17 (Springer Science & Business Media, 2002).
 - [11] R. N. Mantegna and H. E. Stanley, *Introduction to econophysics: correlations and complexity in finance* (Cambridge university press, 1999).
 - [12] <https://www.fidelity.com/learning-center/trading-investing/markets-sectors/global-industry-classification-standard> accessed: 2022-11-22.
 - [13] M. Tumminello, T. Aste, T. Di Matteo, and R. N. Mantegna, A tool for filtering information in complex systems, Proceedings of the National Academy of Sciences **102**, 10421 (2005).
 - [14] T. Aste, T. Di Matteo, and S. Hyde, Complex networks on hyperbolic surfaces, Physica A: Statistical Mechanics and its Applications **346**, 20 (2005).
 - [15] M. Tumminello, T. Di Matteo, T. Aste, and R. N. Mantegna, Correlation based networks of equity returns sampled at different time horizons, The European Physical Journal B **55**, 209 (2007).
 - [16] J.-P. Onnela, K. Kaski, and J. Kertész, Clustering and information in correlation based financial networks, The European Physical Journal B **38**, 353 (2004).
 - [17] <https://wrds-www.wharton.upenn.edu/>.
 - [18] https://osf.io/pfg4w/?view_only=5e8f254160ca4dd7b4703c03c311b6c0.
 - [19] H. Miyahara, H. Qian, P. HOLUR, and V. Roychowdhury, Novel scaling law governing stock price dynamics (2022).
 - [20] R. N. Mantegna, Hierarchical structure in financial markets, The European Physical Journal B-Condensed Matter and Complex Systems **11**, 193 (1999).
 - [21] G. Marti, F. Nielsen, M. Bińkowski, and P. Donnat, A review of two decades of correlations, hierarchies, networks and clustering in financial markets, arXiv preprint arXiv:1703.00485 (2017).
 - [22] D. G. Luenberger *et al.*, Investment science, OUP Catalogue (1997).
 - [23] In the main text, we set $\mu_{\tilde{\gamma}} = 1.0$.
 - [24] T. Vicsek, A. Czirók, E. Ben-Jacob, I. Cohen, and O. Shochet, Novel type of phase transition in a system of self-driven particles, Phys. Rev. Lett. **75**, 1226 (1995).
 - [25] M. Girvan and M. E. J. Newman, Community structure in social and biological networks, Proceedings of the National Academy of Sciences **99**, 7821 (2002), <https://www.pnas.org/doi/pdf/10.1073/pnas.122653799>.
 - [26] T. Vicsek, A. Czirók, E. Ben-Jacob, I. Cohen, and O. Shochet, Novel type of phase transition in a system of self-driven particles, Phys. Rev. Lett. **75**, 1226 (1995).

Appendix E: Author contributions statement

V.R. conceived the experiment(s), H.M., H.Q., P.H. obtained and conducted experiment(s) on the stock market data, V.R., H.M., H.Q., P.H. analysed the empirical results, V.R. H.M. evaluated the generative models. All authors

reviewed the manuscript.

Appendix F: Additional information

The authors declare no competing interests.

Appendix G: Availability of materials and data

Raw S&P 500 stock price data between 2004 and 2020 are available at the Wharton Research Data Services (WRDS) <https://wrds-www.wharton.upenn.edu/>. The repository currently supports over 75000 active researchers over 500 institutions. The code bundle is available on the Open Science Foundation at https://osf.io/pfg4w/?view_only=5e8f254160ca4dd7b4703c03c311b6c0.